



**IJOER**  
RESEARCH JOURNAL

ISSN  
2395-6992

# International Journal of Engineering Research & Science

[www.ijoer.com](http://www.ijoer.com)  
[www.adpublications.org](http://www.adpublications.org)

Volume-6! Issue-5! May, 2020

[www.ijoer.com](http://www.ijoer.com) ! [info@ijoer.com](mailto:info@ijoer.com)

## Preface

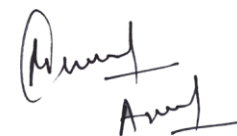
We would like to present, with great pleasure, the inaugural volume-6, Issue-5, May 2020, of a scholarly journal, *International Journal of Engineering Research & Science*. This journal is part of the AD Publications series *in the field of Engineering, Mathematics, Physics, Chemistry and science Research Development*, and is devoted to the gamut of Engineering and Science issues, from theoretical aspects to application-dependent studies and the validation of emerging technologies.

This journal was envisioned and founded to represent the growing needs of Engineering and Science as an emerging and increasingly vital field, now widely recognized as an integral part of scientific and technical investigations. Its mission is to become a voice of the Engineering and Science community, addressing researchers and practitioners in below areas

Chemical Engineering	
Biomolecular Engineering	Materials Engineering
Molecular Engineering	Process Engineering
Corrosion Engineering	
Civil Engineering	
Environmental Engineering	Geotechnical Engineering
Structural Engineering	Mining Engineering
Transport Engineering	Water resources Engineering
Electrical Engineering	
Power System Engineering	Optical Engineering
Mechanical Engineering	
Acoustical Engineering	Manufacturing Engineering
Optomechanical Engineering	Thermal Engineering
Power plant Engineering	Energy Engineering
Sports Engineering	Vehicle Engineering
Software Engineering	
Computer-aided Engineering	Cryptographic Engineering
Teletraffic Engineering	Web Engineering
System Engineering	
Mathematics	
Arithmetic	Algebra
Number theory	Field theory and polynomials
Analysis	Combinatorics
Geometry and topology	Topology
Probability and Statistics	Computational Science
Physical Science	Operational Research
Physics	
Nuclear and particle physics	Atomic, molecular, and optical physics
Condensed matter physics	Astrophysics
Applied Physics	Modern physics
Philosophy	Core theories

Chemistry	
Analytical chemistry	Biochemistry
Inorganic chemistry	Materials chemistry
Neurochemistry	Nuclear chemistry
Organic chemistry	Physical chemistry
Other Engineering Areas	
Aerospace Engineering	Agricultural Engineering
Applied Engineering	Biomedical Engineering
Biological Engineering	Building services Engineering
Energy Engineering	Railway Engineering
Industrial Engineering	Mechatronics Engineering
Management Engineering	Military Engineering
Petroleum Engineering	Nuclear Engineering
Textile Engineering	Nano Engineering
Algorithm and Computational Complexity	Artificial Intelligence
Electronics & Communication Engineering	Image Processing
Information Retrieval	Low Power VLSI Design
Neural Networks	Plastic Engineering

Each article in this issue provides an example of a concrete industrial application or a case study of the presented methodology to amplify the impact of the contribution. We are very thankful to everybody within that community who supported the idea of creating a new Research with IJOER. We are certain that this issue will be followed by many others, reporting new developments in the Engineering and Science field. This issue would not have been possible without the great support of the Reviewer, Editorial Board members and also with our Advisory Board Members, and we would like to express our sincere thanks to all of them. We would also like to express our gratitude to the editorial staff of AD Publications, who supported us at every stage of the project. It is our hope that this fine collection of articles will be a valuable resource for *IJOER* readers and will stimulate further research into the vibrant area of Engineering and Science Research.



Mukesh Arora  
(Chief Editor)

## **Board Members**

### **Mukesh Arora (Editor-in-Chief)**

BE(Electronics & Communication), M.Tech(Digital Communication), currently serving as Assistant Professor in the Department of ECE.

### **Prof. Dr. Fabricio Moraes de Almeida**

Professor of Doctoral and Master of Regional Development and Environment - Federal University of Rondonia.

### **Dr. Parveen Sharma**

Dr Parveen Sharma is working as an Assistant Professor in the School of Mechanical Engineering at Lovely Professional University, Phagwara, Punjab.

### **Prof.S.Balamurugan**

Department of Information Technology, Kalaignar Karunanidhi Institute of Technology, Coimbatore, Tamilnadu, India.

### **Dr. Omar Abed Elkareem Abu Arqub**

Department of Mathematics, Faculty of Science, Al Balqa Applied University, Salt Campus, Salt, Jordan, He received PhD and Msc. in Applied Mathematics, The University of Jordan, Jordan.

### **Dr. AKPOJARO Jackson**

Associate Professor/HOD, Department of Mathematical and Physical Sciences, Samuel Adegboyega University, Ogwa, Edo State.

### **Dr. Ajoy Chakraborty**

Ph.D.(IIT Kharagpur) working as Professor in the department of Electronics & Electrical Communication Engineering in IIT Kharagpur since 1977.

### **Dr. Ukar W.Soelistijo**

Ph D , Mineral and Energy Resource Economics, West Virginia State University, USA, 1984, Retired from the post of Senior Researcher, Mineral and Coal Technology R&D Center, Agency for Energy and Mineral Research, Ministry of Energy and Mineral Resources, Indonesia.

### **Dr. Samy Khalaf Allah Ibrahim**

PhD of Irrigation &Hydraulics Engineering, 01/2012 under the title of: "Groundwater Management Under Different Development Plans In Farafra Oasis, Western Desert, Egypt".

### **Dr. Ahmet ÇİFCİ**

Ph.D. in Electrical Engineering, Currently Serving as Head of Department, Burdur Mehmet Akif Ersoy University, Faculty of Engineering and Architecture, Department of Electrical Engineering (2015-...)

### **Dr. Mohamed Abdel Fatah Ashabrawy Moustafa**

Ph.D. in Computer Science - Faculty of Science - Suez Canal University University, 2010, Egypt.

Assistant Professor Computer Science, Prince Sattam bin AbdulAziz University ALkharj, KSA.

### **Dr. Heba Mahmoud Mohamed Afify**

Ph.D degree of philosophy in Biomedical Engineering, Cairo University, Egypt worked as Assistant Professor at MTI University.

### **Dr. Aurora Angela Pisano**

Ph.D. in Civil Engineering, Currently Serving as Associate Professor of Solid and Structural Mechanics (scientific discipline area nationally denoted as ICAR/08—"Scienza delle Costruzioni"), University Mediterranea of Reggio Calabria, Italy.

### **Dr. Faizullah Mahar**

Associate Professor in Department of Electrical Engineering, Balochistan University Engineering & Technology Khuzdar. He is PhD (Electronic Engineering) from IQRA University, Defense View, Karachi, Pakistan.

### **Dr. S. Kannadhasan**

Ph.D (Smart Antennas), M.E (Communication Systems), M.B.A (Human Resources).

### **Dr. Christo Ananth**

Ph.D. Co-operative Networks, M.E. Applied Electronics, B.E Electronics & Communication Engineering Working as Associate Professor, Lecturer and Faculty Advisor/ Department of Electronics & Communication Engineering in Francis Xavier Engineering College, Tirunelveli.

### **Dr. S.R.Boselin Prabhu**

Ph.D, Wireless Sensor Networks, M.E. Network Engineering, Excellent Professional Achievement Award Winner from Society of Professional Engineers Biography Included in Marquis Who's Who in the World (Academic Year 2015 and 2016). Currently Serving as Assistant Professor in the department of ECE in SVS College of Engineering, Coimbatore.

### **Dr. Maheshwar Shrestha**

Postdoctoral Research Fellow in DEPT. OF ELE ENGG & COMP SCI, SDSU, Brookings, SD  
Ph.D, M.Sc. in Electrical Engineering from SOUTH DAKOTA STATE UNIVERSITY, Brookings, SD.

### **Zairi Ismael Rizman**

Senior Lecturer, Faculty of Electrical Engineering, Universiti Teknologi MARA (UiTM) (Terengganu) Malaysia  
Master (Science) in Microelectronics (2005), Universiti Kebangsaan Malaysia (UKM), Malaysia. Bachelor (Hons.) and Diploma in Electrical Engineering (Communication) (2002), UiTM Shah Alam, Malaysia

### **Dr. D. Amaranatha Reddy**

Ph.D.(Postdoctoral Fellow,Pusan National University, South Korea), M.Sc., B.Sc. : Physics.

## **Dr. Dibya Prakash Rai**

Post Doctoral Fellow (PDF), M.Sc.,B.Sc., Working as Assistant Professor in Department of Physics in Pachhunga University College, Mizoram, India.

## **Dr. Pankaj Kumar Pal**

Ph.D R/S, ECE Deptt., IIT-Roorkee.

## **Dr. P. Thangam**

BE(Computer Hardware & Software), ME(CSE), PhD in Information & Communication Engineering, currently serving as Associate Professor in the Department of Computer Science and Engineering of Coimbatore Institute of Engineering and Technology.

## **Dr. Pradeep K. Sharma**

PhD., M.Phil, M.Sc, B.Sc, in Physics, MBA in System Management, Presently working as Provost and Associate Professor & Head of Department for Physics in University of Engineering & Management, Jaipur.

## **Dr. R. Devi Priya**

Ph.D (CSE),Anna University Chennai in 2013, M.E, B.E (CSE) from Kongu Engineering College, currently working in the Department of Computer Science and Engineering in Kongu Engineering College, Tamil Nadu, India.

## **Dr. Sandeep**

Post-doctoral fellow, Principal Investigator, Young Scientist Scheme Project (DST-SERB), Department of Physics, Mizoram University, Aizawl Mizoram, India- 796001.

## **Mr. Abilash**

MTech in VLSI, BTech in Electronics & Telecommunication engineering through A.M.I.E.T.E from Central Electronics Engineering Research Institute (C.E.E.R.I) Pilani, Industrial Electronics from ATI-EPI Hyderabad, IEEE course in Mechatronics, CSHAM from Birla Institute Of Professional Studies.

## **Mr. Varun Shukla**

M.Tech in ECE from RGPV (Awarded with silver Medal By President of India), Assistant Professor, Dept. of ECE, PSIT, Kanpur.

## **Mr. Shrikant Harle**

Presently working as a Assistant Professor in Civil Engineering field of Prof. Ram Meghe College of Engineering and Management, Amravati. He was Senior Design Engineer (Larsen & Toubro Limited, India).

## Table of Contents

S.No	Title	Page No.
1	<p><b>Robust Gesture Recognition Based on Embedded System</b>  <b>Authors:</b> FeiWang, Yanli Dong, Hui Yang, Feiyan Zhao</p> <p> DOI: <a href="https://dx.doi.org/10.5281/zenodo.3868973">https://dx.doi.org/10.5281/zenodo.3868973</a></p> <p> <b>DIN</b> Digital Identification Number: IJOER-MAY-2020-3</p>	01-06
2	<p><b>Experimental study on four rotor helicopter 10 m-range distance and position measurement method by using two searchlights for autonomous control and the evaluation</b>  <b>Authors:</b> Hideki Toda</p> <p> DOI: <a href="https://dx.doi.org/10.5281/zenodo.3869071">https://dx.doi.org/10.5281/zenodo.3869071</a></p> <p> <b>DIN</b> Digital Identification Number: IJOER-MAY-2020-6</p>	07-15
3	<p><b>Parametric Analysis of Interlaminar Toughness of Unidirectional Carbon Fiber and Woven Carbon Fabric Composites</b>  <b>Authors:</b> Panagiotis J. Charitidis</p> <p> DOI: <a href="https://dx.doi.org/10.5281/zenodo.3869119">https://dx.doi.org/10.5281/zenodo.3869119</a></p> <p> <b>DIN</b> Digital Identification Number: IJOER-MAY-2020-7</p>	16-26
4	<p><b>Tilapia Powered Aquaponics to Optimize Land and Water Use for Safe Food Production from the Rooftop</b>  <b>Authors:</b> M. A. Salam, Tania Islam, Zubyda Mushtari Nadia</p> <p> DOI: <a href="https://dx.doi.org/10.5281/zenodo.3883754">https://dx.doi.org/10.5281/zenodo.3883754</a></p> <p> <b>DIN</b> Digital Identification Number: IJOER-MAY-2020-8</p>	27-36
5	<p><b>Analysis of Air Conditioning Schemes based on Evaporative Cooling of Air using Solar Energy</b>  <b>Authors:</b> Toshmamatov B.M., Temirova L.Z., Baratova S.R., Safarova S.U., Khusunov Sh.Kh.</p> <p> DOI: <a href="https://dx.doi.org/10.5281/zenodo.3883758">https://dx.doi.org/10.5281/zenodo.3883758</a></p> <p> <b>DIN</b> Digital Identification Number: IJOER-MAY-2020-9</p>	37-41

# Robust Gesture Recognition Based on Embedded System

Fei Wang<sup>1</sup>, Yanli Dong<sup>2</sup>, Hui Yang<sup>3</sup>, Feiyan Zhao<sup>4</sup>

Zhejiang University Kunshan Innovation Institute, Kunshan 215300, China

**Abstract**— To improve portability of current gesture recognition technology, this paper proposes a method of the design and implementation of gesture recognition based on embedded system by combining embedded platform with Open CV. Firstly, image denoising using the weighted mean filtering method, and the morphological open operation is used to obtain the complete contour, and the edge extraction is carried out by the improved Canny operator; Secondly, image segmentation using two-dimensional maximum interclass variance. Then analysis and processing of specifies the feature information of gestures images using Hu distance. Finally, the template matching method is used to recognize the gesture image. The experimental results show that the gesture recognition based on embedded system has strong portability, higher recognition rate and easy implementation.

**Keywords**— *Embedded, template matching, human-computer interaction, Hu distance.*

## I. INTRODUCTION

Gesture recognition is one of the most intuitive forms of human-computer interface. It has gradually become a hot spot in many scientific fields. At present, the research on gesture recognition technology is mainly focused on the two aspects of vision and sensor hardware [1,2,3]. Gesture recognition based on sensor acceleration hardware requires the help of some hardware equipment to complete the operation; such equipment is expensive, not easy to wear. Furthermore, that needs to be used in a specific situation, the limitations are very large [4,5].

For gesture recognition based on visual information, it is only necessary to complete the communication between man and machine through human gesture action without intermediate media. It makes gesture recognition convenient and effective because of no external device. And then it brings users a new interactive experience and freedom. Dynamic gestures are one of the most intuitive and effective approach for human-computer interaction [6,7,8,9]. Therefore, we present gesture recognition based on embedded system in order to better recognize and obtain gesture information. The gestures images are acquired by camera are preprocessed, and then the gesture features are extracted and recognized.

## II. IMAGE PREPROCESSING

### 2.1 Gesture image denoising

The weighted mean filtering algorithm is also called linear filtering, which is neighborhood averaging method that is using the average value of several pixels gray to replace the gray level of each pixel [10]. General definition of weight filtering is defined as follow:

$$W_{mean} \{I(x, y)\} = \sum_{(x,y) \in \Omega_{i,j}} w(x, y) \times I(x, y) \quad (1)$$

Then the weight value in the filter template is the reciprocal of the Euclidean distance, which is defined as follow:

$$w_0(x, y) = 1 / \sqrt{\sum_{(x,y) \in \Omega_{i,j}} [(x - x_0)^2 + (y - y_0)^2]} \quad (2)$$

Where  $(x_0, y_0)$  is the position coordinate of the central pixel point. Then the Weight normalized is defined as follow:

$$w(x, y) = w_0(x, y) / \sum_{x,y \in \Omega_{i,j}} w_0(x, y) \quad (3)$$

### 2.2 Morphological image processing

The morphological opening operation is used to extract the components of the gesture image, which effectively preserves the details of the original image and the basic shape features. The opening operation is defined as follow:

$$A \circ B = (A \ominus B) \oplus B \quad (4)$$

A is defined target image. B is defined structural element. Operation can separate some adhesion targets, which is very significant for removing salt and pepper noise.

### 2.3 Image threshold segmentation

The maximum between-Cluster variance is derived based on the principle of decision analysis or least square method, which is proposed by the great progress of Japan, also known as the Otsu threshold [11,12]. The maximum between-Cluster variance is defined as follow:

$$\sigma_T^2 = w_A w_B (u_A - u_B)^2 \quad (5)$$

Changing the t value until  $\sigma_T^2$  is the maximum, then T is the optimal segmentation threshold.

### 2.4 Image edge detection

For a good edge detection algorithm, it should have three basic conditions: high positioning accuracy, low error rate and suppression of false edges. Candy operator proposed three optimization criteria for these three conditions [13]: maximum noise ratio criterion, optimal zero-crossing positioning criterion and multi-peak response criterion. The implementation steps are as follows:

- Image denoising by Gaussian filter;
- Using the first order partial derivative finite difference to find the direction and amplitude of the gradient; The function is defined as follow:

$$F(x, y) = \sqrt{F_1^2(x, y) + F_2^2(x, y)} \quad (6)$$

$$G_F = \arctan \frac{F_2(x, y)}{F_1(x, y)} \quad (7)$$

Where F is amplitude of the image gradient.  $G_F$  is Direction of the image.

- Finding the maximum of the image gradient;
- Using double threshold algorithm to discriminate and connect for the edges.

A large amount of noise can be effectively eliminated and the edge contrast of the image can be enhanced by improving the original operator.

## III. GESTURE FEATURE EXTRACTION AND RECOGNITION

### 3.1 Hu invariant moment

The image is preprocessed by the above algorithm to extract the features of the image. The Hu invariant moments are used to extract the features of gesture images since the Hu invariant moments have the invariance of translation, rotation and scaling [14]. Calculating the similarity of the contour between the two images by Hu invariant moment, then the value with high degree of acquaintance is chosen as the recognition criterion. Feature extraction using Hu distance can ensure that some feature quantities of the image remain unchanged in size, position and direction, and then improve the accuracy of gesture recognition [15,16]. The seven moment invariants are used to describe the important features in the image that want to extract the target region. Then the functions are defined as follow:

$$\begin{aligned} \omega_1 &= v_{20} + v_{02} \\ \omega_2 &= (v_{20} - v_{02})^2 + 4v_{11}^2 \\ \omega_3 &= (v_{30} - 3v_{12})^2 + (3v_{21} - v_{03})^2 \\ \omega_4 &= (v_{30} + v_{12})^2 + (v_{21} + v_{03})^2 \\ \omega_5 &= (v_{30} - 3v_{12})(v_{30} + v_{21})[(v_{30} + v_{12})^2 - 3(v_{21} - v_{03})^2] \\ &+ (3v_{21} - v_{03})(v_{21} + v_{03})[3(v_{30} + v_{12})^2 - (v_{21} + v_{03})^2] \\ \omega_6 &= (v_{20} - v_{02})[(v_{30} + v_{21})^2 - (v_{21} + v_{03})^2] + 4v_{11}(v_{30} + v_{12})(v_{21} + v_{03}) \\ \omega_7 &= (3v_{21} - v_{03})(v_{30} + v_{12})[(v_{30} + v_{12})^2 - 3(v_{21} + v_{03})^2] \\ &- (v_{30} - 3v_{12})(v_{21} + v_{03})[3(v_{30} + v_{12})^2 - (v_{21} + v_{03})^2] \end{aligned} \quad (8)$$

### 3.2 BP neural network

BP neural network [17] is a kind of multi-layer feed forward neural network. Then the threshold and weights are trained by error propagation algorithm to reduce the error between layers and realized the given mapping relationships before and after. The structures consist of an input layer, one or more hidden layers, and an output layer. The network structure is shown in fig 1. The learning process consists of a forward and backward propagation process. Forward propagation is that the input information is processed layer by layer from the input layer to one or more hidden layers, and then to the output layer. Backpropagation is that the error of the output is returned according to the original path when the expected output value is not reached, then the weight between the layers is calculated layer by layer to minimize the error. Gradient descent algorithm is used to train the network. The Sigmoid function is made as the activation function in order to ensure the differentiability of the function.

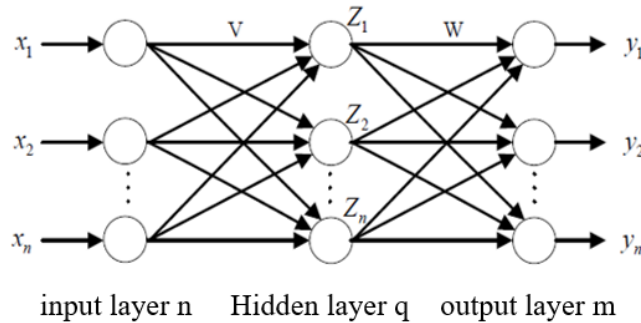


**FIGURE 1: BP neural network**

## IV. SYSTEM DESIGN AND REALIZATION

### 4.1 Introduction to Hardware and Software

#### 4.1.1 System software environment

- 1) PC operating system: Fedora14, Windows XP.
- 2) Virtual machines: VMware-6.5.1.
- 3) Graphic interface development tools: Qtopia2.2.0.
- 4) Open source computer visual library: OpenCV2.4.3.

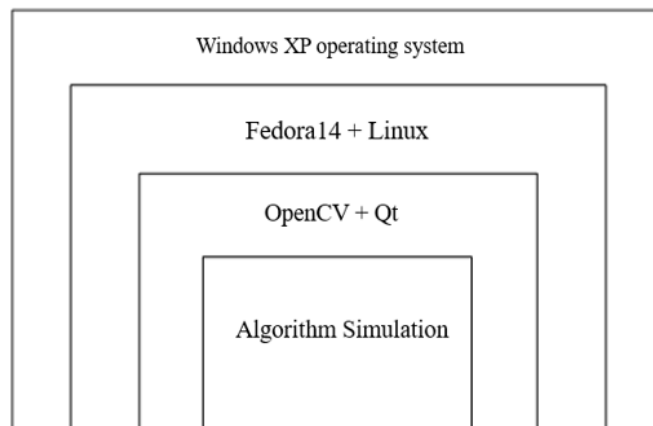


**FIGURE 2. The system software diagram**

#### 4.1.2 System hardware environment

- 1) PC hardware configuration: core i5CPU, 2G running memory, 3.19 GHz main frequency.
- 2) ARM development board configuration: CPU processor Samsung s3c2440A, master frequency 400 MHz, 64M SDRAM memory, 3.5 inch touch screen.
- 3) Camera configuration: USB2.0 interface.
- 4) FLASH storage :256 M/1GB Nand Flash, 2M Nor Flash.

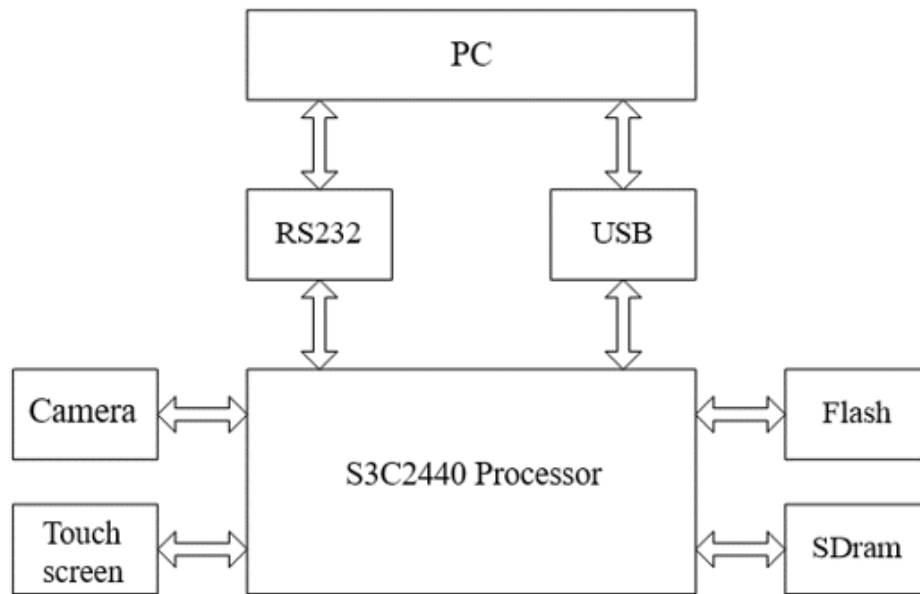


**FIGURE 3. The system hardware diagram**

**4.2 Gesture recognition experiment and analysis**

In this study, The Hu invariant moments of the gesture template are compared with the Hu invariant moments of the current acquisition gesture from the camera, then the similar Hu invariant moments value is used as the criterion of gesture recognition. Fig 4 is a template for ten kinds of gesture images. Fig 5 is the contour image of ten kinds of gesture templates.

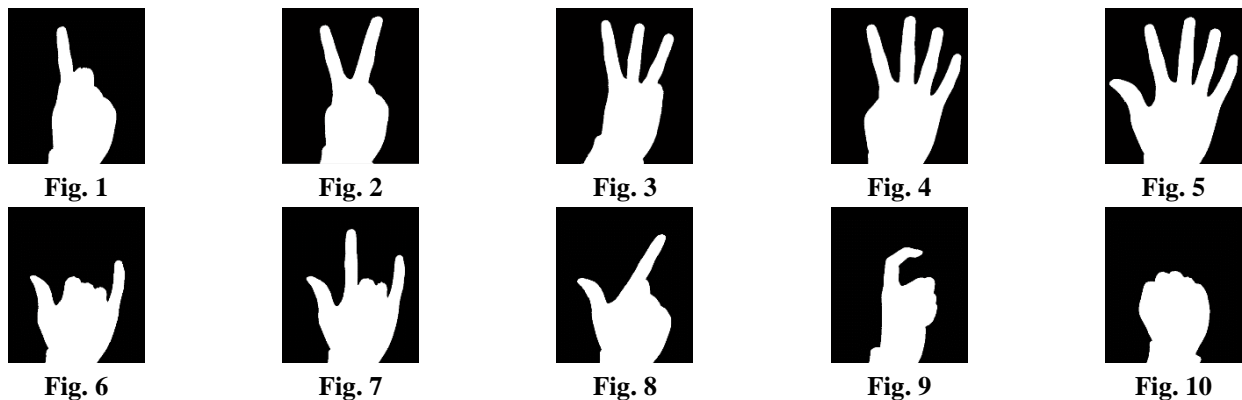


**FIGURE 4: Ten kinds of gesture templates**

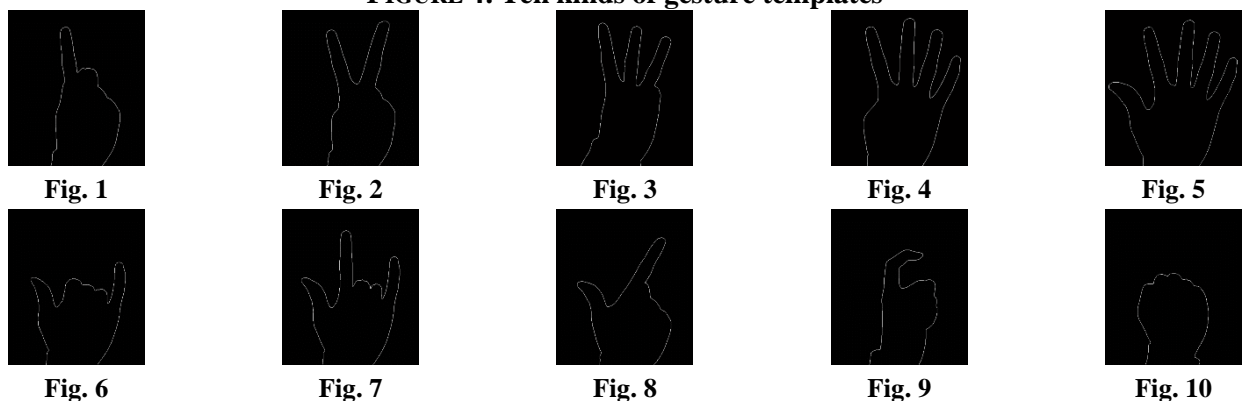


**FIGURE 5: Ten kinds of gesture contours**

In both simple and complex background, the gesture video is detected and recognized by the embedded development board, and then the number of gestures is given. This paper lists three kinds of gesture recognition effects: three, five, eight as shown in the following fig 6,7:



**FIGURE 6: Under the simple background gestures rendering**

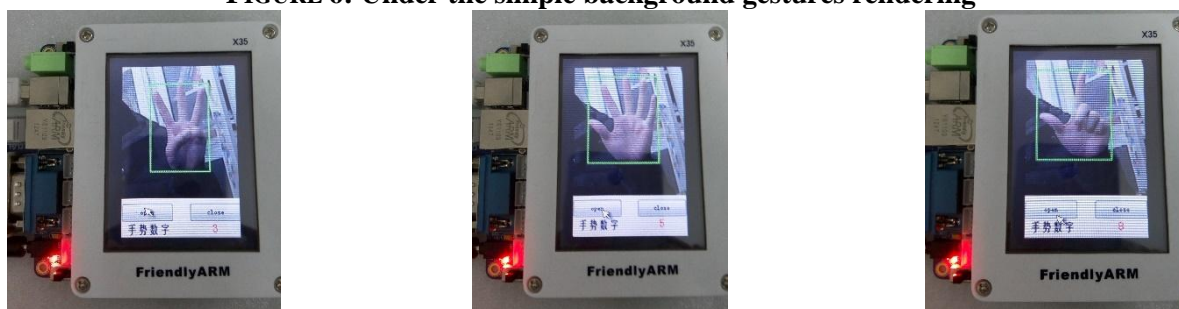


**FIGURE 7: Under complicated background rendering**

One hundred images were randomly collected for each gesture to identify in order to verify the effectiveness and practicability of the gesture recognition system. Then the recognition rate of each gesture before and after the improvement of the BP neural network algorithm was obtained.

**TABLE 1  
TEN KINDS OF GESTURE RECOGNITION RATE UNDER DIFFERENT BACKGROUND**

Data set	Original algorithm		Improved algorithm	
	In a simple background	In a complex background	In a simple background	In a complex background
1	83%	75%	96%	92%
2	79%	70%	93%	90%
3	81%	73%	90%	87%
4	76%	69%	93%	88%
5	79%	75%	96%	91%
6	80%	70%	92%	89%
7	78%	68%	91%	86%
8	85%	74%	94%	90%
9	73%	65%	90%	85%
10	86%	80%	97%	93%

From Table1, it can be seen that the gesture recognition rate in different backgrounds is increased by 16% and 23% respectively compared with the previous one by improving the algorithm. The gesture recognition rates are also different in different background. The recognition rate is higher in simple background. The recognition rate is reduced in complex background. The different light intensity and the similarity of each gesture cause the final effect of gesture recognition. When extracting gesture features in a complex background, it will affect the Hu moments value of the gesture, resulting in a large difference between the Hu moments value and the template, which will affect the recognition rate of the whole system. The characteristic value and quality of various gesture images are so stable that the recognition rate of gesture system is higher in simple background.

To sum up, through a large number of experiments, it can be seen that the whole gesture recognition system has a good recognition effect, which can meet the basic application requirements and also confirms the reliability and practicability of the gesture recognition system.

## V. CONCLUSION

At present, many gesture recognition techniques have been applied to PC machines, resulting in great limitations, poor portability and practicability. Therefore, this paper realizes the embedded gesture recognition system by using the combination of embedded system and image processing technology based on the existing gesture recognition technology. Video stream is collected by USB camera, then different gesture commands are obtained to achieve human-computer interaction through gesture processing in the video stream. Finally, the whole gesture recognition system is verified to ensure that the whole system is real-time and effective.

## REFERENCES

- [1] V. Pavlovic, R. Sharma, T. Huang. Visual Interpretation of Hand Gestures for Human-Computer Interaction[J]. IEEE Transaction on Pattern Analysis and Machine Intelligence. 1997, 9(7): 677-695.
- [2] Y. Wu, T. Huan. Vision-based Gesture Recognition[A]. France: Proceedings of the International Gesture Recognition Workshop. 2009, 4(9): 73-79.
- [3] Hardenberg CV, Berard F. Bare-Hand human-computer interaction[C]. In: Proc. of the ACM workshop on Perceptual User Interface, 2001: 15-17.
- [4] RenqiangXie, Juncheng Cao. Accelerometer-Based Hand Gesture Recognition by Neural Network and Similarity Matching[J]. IEEE Sensors Journal. 2016, 4537-4545.
- [5] S. Hazra, A. Santra. Robust Gesture Recognition Using Millimetric-Wave Radar System[J]. IEEE Sensors Letters. 2018,1-4.
- [6] W. Fang, Y. Ding, F. Zhang and J. Sheng. Gesture Recognition Based on CNN and DCGAN for Calculation and Text Output[J]. IEEE Access. 2019,28230-28237.
- [7] G. Plouffe and A. Cretu. Static and Dynamic Hand Gesture Recognition in Depth Data Using Dynamic Time Warping[J]. IEEE Transactions on Instrumentation and Measurement. 2016, 305-316.
- [8] R. Xie, X. Sun, X. Xia and J. Cao. Similarity Matching-Based Extensible Hand Gesture Recognition[J]. IEEE Sensors Journal. 2015, 3475-3483.
- [9] G. Li, H. Wu, G. Jiang, S. Xu and H. Liu. Dynamic Gesture Recognition in the Internet of Things[J]. IEEE Access.2019, 23713-23724.
- [10] NeelaChithirala, Natasha. B, Rubini. N. Weighted Mean Filter for Removal of High Density Salt and Pepper Noise[J]. International Conference on Advanced Computing and Communication Systems. 2016,22-23.
- [11] Wesley E. Snyder and Hairong Qi, Machine vision[M]. China Machine Press. 2005.
- [12] A. Thayananthan, B Stenger, PHS. Torr, R Cipolla. Shape Context and Chamfer Matching in Cluttered Scenes[J]. IEEE Computer Society Conference on Computer Vision and Pattern Recogniyion.2003: 1-8.
- [13] A P Tzannes, D H Brooks. Detection of point targets in image sequences by hypothesis testing a temporal test first approach[J]. IEEE. Proc. 2000, 39(39): 2270-2278.
- [14] SouvikHazra, AvikSantra. Robust Gesture Recognition Using Millimetric-Wave Radar System[J]. IEEE. 2017.
- [15] S Mckenna, S Jabri, Z Duric, A Rosenfeld, H Wechsler. Tracking groups of people activities[J]. IEEE Trans. On Pattern Analysis and Machine Intelligence. 2002, 22(8): 809-830.
- [16] S Mckenna, S Jabri, Z Duric, A Rosenfeld, H Wechsler. Tracking groups of people activities[J]. IEEE Trans. On Pattern Analysis and Machine Intelligence. 2002, 22(8): 809-830.
- [17] Y. Cao and L. Zhang. Data fusion of heterogeneous network based on BP neural network and improved SEP[J]. International Conference on Advanced Infocomm Technology (ICAIT). 2017, 138-142.

# Experimental study on four rotor helicopter 10 m-range distance and position measurement method by using two searchlights for autonomous control and the evaluation

Hideki Toda

Department of Electric and Electronic Engineering, University of Toyama, Japan, Gofuku 3190

**Abstract**—This paper reports experimental result of a distance and position measurement method for autonomous movement control of four-rotor helicopters (drones) that uses two spotlights and comparing with a red marker using case, discuss the results of autonomous flight test evaluations. To conduct autonomous drone flights exceeding 10 m under unstable GPS signal situations, such as under bridges or inside tunnels during periodic maintenance inspections, correct self-positioning measurements are indispensable. This study proposes a simple method whereby autonomous drone movement control can be performed over distances exceeding 10 m by using two high-power 100 V alternating current spotlights set on the ground as infrared (IR) light sources. The spotlights are directed at the investigation target, such as the cracked area of a bridge, and the intense light of the two spotlights provides reference points that enable the drone to determine its correct position. In autonomous flight-testing in an enclosed corridor, our method provides capable of determining the drone's position at distances up to 15 m with a standard deviation of 0.31 m. Our proposed method would be effective in situations where no skilled drone control operator is available and for flights requiring visual cue confirmations under adverse outdoor conditions.

**Keywords**—Infrared spotlights, Four-rotor helicopter, Long distance measurements, Bridge/tunnel investigations.

## I. INTRODUCTION

In this paper, a distance and position measurement method for autonomous movement control of four-rotor helicopters (drones) that uses two spotlights and discuss the results of a related autonomous flight test evaluation. To achieve drone flights in excess of 10 m under unstable global positioning system (GPS) signal situations, such as under bridges or inside tunnels and buildings during periodic maintenance inspections, an easy and precise self-positioning measurement method is indispensable for stable control [1,2]. This is because, even if a drone is human controlled, it is difficult for an operator to manipulate the device in flight at distances in excess of 10 m using visual cues alone [3-12]. In those situations, other supporting mechanisms are necessary for drone control and position measurements [3,4,13-26]. The aim of this study is to propose a simple method whereby autonomous drone movement control can be performed over distances exceeding 10 m by using two high-power 100 V alternating current (AC) spotlights set on the ground as infrared (IR) light sources (Fig. 1) and it is comparing with the general method of using a red colored marker board attached to the drone. In our method, the spotlights are directed at the investigation target position, such as the cracked area on the side of a bridge [2].

Since drone helicopters are seldom equipped with internal autonomous position controls, ground-based positioning systems based on IR light sources, three-dimensional (3D) cameras, or GPS sensors are needed control their positions during flight [10,11,22-28]. In the case of methods using IR or 3D cameras, the position measurement precision can be on the order of 1 mm, but these methods are normally restricted to indoor situations at distances less than 10 m [5,13]. On the other hand, if a drone is being controlled in an outdoor situation, GPS signals can be used as long as there are limited numbers of obstacles in the skyward and movement directions. However, when using a drone for periodic inspection under bridges or inside tunnels, neither of the abovementioned two approaches can be adopted because distances tend to be excessive and GPS signal reception under bridges or within tunnels is often unstable [2]. If a drone position is detected based on visual cues, cameras can be used to measure its position. This is known as visual-servo control [26-29]. However, in situations where there are numerous obstacles in the camera image, it is difficult for the controlling operator to ascertain a drone's position based on camera imagery alone, especially at distances in excess of 10 m from the starting point.

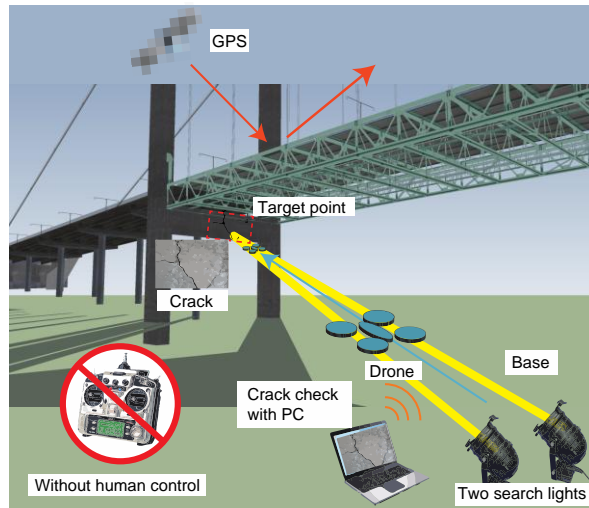


**FIGURE 1: Proposed distance measurement method for autonomous drone flights at distances in excess of 10 m using two high-power 100 V AC spotlights set on the ground**

**II. METHODS**

A basic overview of the proposed method is shown in Fig.2. Two high-power spotlights (Stage Evolution, PAR56SBG equipped with 16 cm diameter Sylvania PAR56 300W halogen lamps, Sound House Corp.) were used to provide ground-based IR light sources. A 320 × 240 pixel, 30 frame per second (fps) quarter video graphics array (QVGA) camera (Trek 2000, Ai-ball) mounted at the front of the drone was aligned in the direction of the two spotlights and controlled by using the positions of those spotlights on the camera image based on the center of gravity (CoG) of two points using simple proportional control. An IR filter (IR76, Fuji Filter, Fujifilm Corp.) was mounted on the front of the camera lens. The Ai-ball wireless camera was selected due to the excessively large time delay of the drone's internal camera imagery and control command transmissions (>around 100 msec). Since the Ai-ball camera was positioned at the front of the drone, the drone moved in the backward direction when approaching to the target position. Drone control was provided by the ARDroneForP5 library (Y. Shigeo) control suite [30].

To estimate the drone position, the spotlight positions were extracted from the camera image. An example image is shown in the middle of the right side of Fig. 2(c). The green extracted image areas are approximately 10 pixels wide when the drone is 15 m away from the lights.

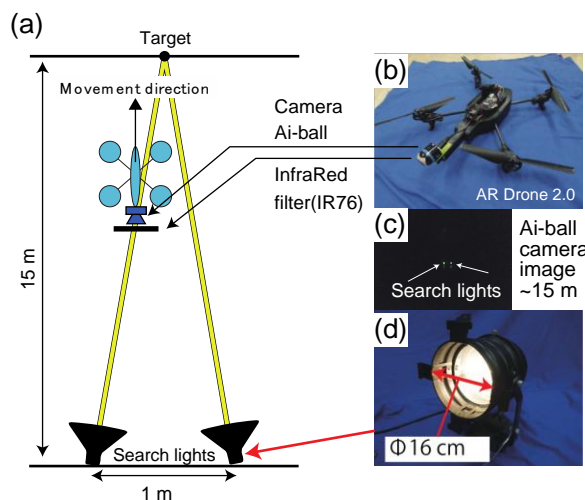


**FIGURE 2: Basic concept of drone 10+ m range position measurement method. (a) Two spotlights (PAR56BSG, Stage Evolution) were used to provide IR light sources for in-flight drone position measurements. (b) Using drone system (A.R.Drone 2.0). (c) Search light positions in the camera image. (d) Using spot light.**

### III. EXPERIMENT

#### 3.1 Experiment 1: Condition of red fluorescent marker attached to drone facing rearward

Drone position estimations have been commonly performed via techniques such as IR light reflection marker(s) or red marker(s) attached to the drone [3,4,10,13]. Marker positions are captured by camera(s) installed in the environment. The conventional method used in Experiment 1 confirmed the stability of drone's position measurement by means of a single red fluorescent marker attached to the rearward facing side (5065 fluorescent sheet red, Myst Corp.) (Fig. 3) of the drone during a 15 m autonomous movement control experiment in an enclosed university corridor. The drone position was determined by using the red fluorescent marker attached to the rearward facing side of the drone via the view from a fixed camera located on the ground. The flight time was 50 sec. Various sized red fluorescent markers (100 × 100, 150 × 150, 200 × 200 mm) and 320 × 240 pixels, 30 fps fixed camera (C270, Logicool Corp.) were used for the position measurements in this experiment.

For the control method, when the CoG of the red fluorescent target marker (Fig. 4a) is  $(G_x, G_y)$  and the area is A in the fixed camera image, the drone's movement roll and pitch speed commands  $V_{command}^r$ ,  $V_{command}^p$  were described as,

$$\begin{aligned} V_{command}^r &= \gamma_r (160 - G_x) \\ V_{command}^p &= \gamma_p \end{aligned} \quad (1)$$

Where the meaning of  $\gamma_r, \gamma_p$  are constants. Simple proportional feedback was used in the experiment.  $\gamma_p$  used the drone on a 10% constant forward movement setting. The  $\gamma_r$  feedback parameters were determined by 30 sec continuously measured flight control experiments ( $N > 100$  times) in order to minimize the standard deviation (SD) of  $G_x$ . The sign for parameter  $\gamma_p$  was changed when the drone approached the target distance of approximately 15 m (23 sec of flight time). The distance z from the camera was calculated from the conversion function  $= g(A) \sim \frac{\alpha}{\sqrt{A}}$ , which had been previously measured by using a geometric layout of the camera and Area A. The control command sending speed was approximately 100 msec since it is the limit of communication speed (command sending) of the drone used in our experiment. The rotational (yaw) direction was slightly changed ( $< 1^\circ$ ) after 50 sec of controlled flight and the height of the above from the ground was maintaining at approximately 0.8 m via the drone control mechanism ( $G_y$  was not used in the experiment). This type of visual servo system has been adopted in many remote-control aircraft control procedures, including four-rotor drones [13-15].

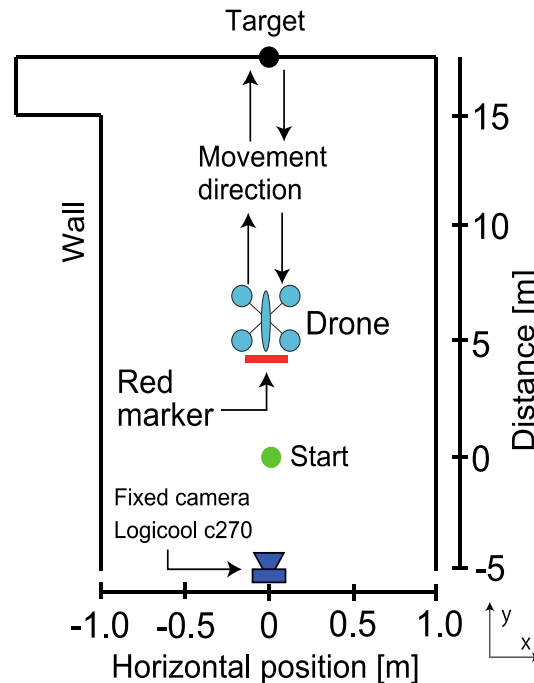


**FIGURE 3: Experiment 1 setup for 15 m autonomous movement control experiment in an enclosed corridor (conventional method) using various sized red fluorescent markers (100×100, 150×150, 200×200 mm) attached to the drone facing rearward.**

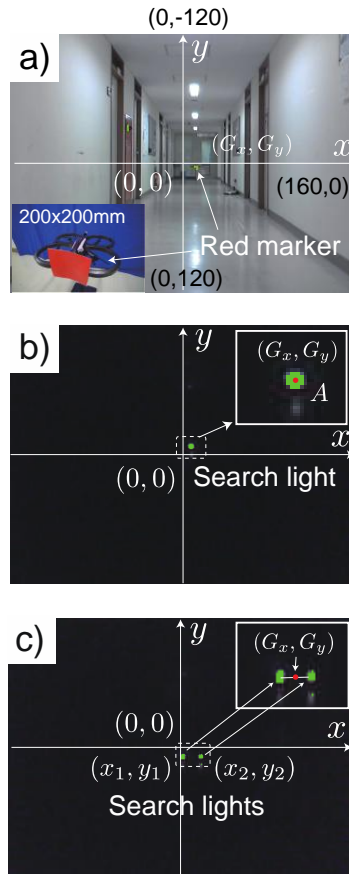


**FIGURE 4: Camera image axis definition and image processing examples in the case of (a) 200×200 mm red fluorescent color and (b) single, (c) IR light intensity of two spotlights when the drone was positioned 15 m from the start position. The green areas show extracted red marker positions or IR luminance areas.**

### 3.2 Experiment 2 and 3: Conditions for single or two IR spotlights positioned on the ground

In the following experiments, which were conducted to evaluate our proposed method, the spotlights(s) were used to measure the position of the drone instead of a red marker. The position of the drone could be calculated from the CoG of a "single" spotlight position  $\vec{x}_1 = (x_1, y_1)$  and spotlight luminance Area A on the camera image (Fig. 4b). The horizontal and vertical position (x-y axis) of the drone is  $\vec{x}_1$  and the distance z from the camera is calculated from the conversion function  $z = g(A) \sim \frac{a}{\sqrt{A}}$ , which had been previously measured by using the geometric layout of the camera and Area A.

However, the drone position could also be calculated from the CoG positions of two spotlights  $\vec{x}_1 = (x_1, y_1)$   $\vec{x}_2 = (x_2, y_2)$  on the camera image (Fig. 4c).  $\vec{x}_0 = (\vec{x}_1 + \vec{x}_2)/2$  represents the horizontal and vertical position (x-y axes) of the drone. The rotation  $\theta$  in the x-y plane was calculated from  $\tan\theta = (y_2 - y_1)/(x_2 - x_1)$ , and the distance z from the camera was calculated from  $l = |\vec{x}_2 - \vec{x}_1|$  and the conversion function  $z = f(l)$ , which had been previously measured using the geometric layout of the camera and the markers.

In Experiments 2 and 3, the two drone position measurement methods mentioned above were compared. The experimental setup is shown in Fig. 5. Here, the measurement stability of the distance z in cases when a single spotlight is used (Experiment 2) and cases when two spotlights are used (Experiment 3) is evaluated as the drone is traveling to a target 15 m away (0,15) and returning to the start position (0,0). In the single spotlight case (Experiment 2), the spotlight was positioned at (0, -5). The green dot represents the start position and the two yellow dots are the spotlight position. In Experiment 3, the two spotlights were positioned at (-0.5, -5) and (0.5, -5) m relative to the drone flight start position of (0,0).

As with Experiment 1, the QVGA camera attached in the front of the drone was used for real-time position information measurement and control was performed based on the position and area of the target object (spotlight image) in the camera image within a 100 msec period.

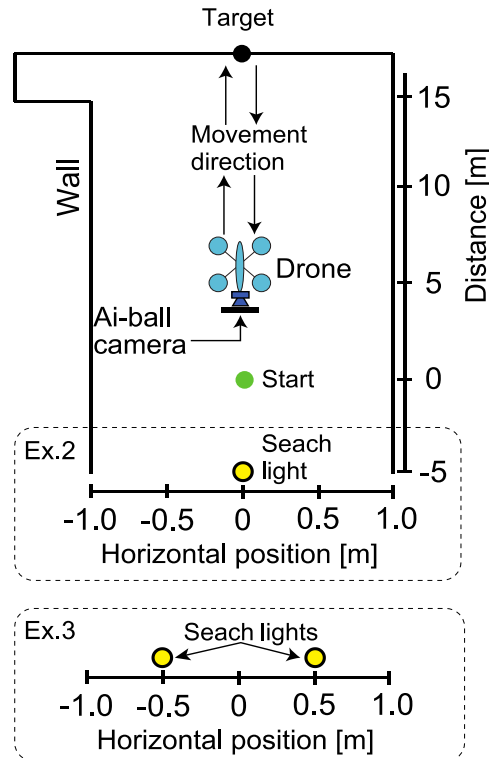


**FIGURE 5: 15 m autonomous movement control distance experimental setup using single (Experiment 2) and two (Experiment 3) spotlights in an enclosed corridor**

When the center of the two spotlight positions is  $\vec{x}_0 = \frac{\vec{x}_1 + \vec{x}_2}{2} = (G_x, G_y)$ , the drone's movement roll and pitch speed commands  $V_{command}^r, V_{command}^p$  were same with Eq. (1). Simple proportional feedback was used in the experiment. They  $\gamma_p$  used the 10% constant forward movement settings of the drone. The  $\gamma_r$  feedback parameters were determined using the same procedure as Experiment 1. The sign of parameter  $\gamma_p$  was changed when the drone reached the target distance of approximately 15 m (approximately 23 sec flight time).

### 3.3 Experiment 4: 15 m range round trip movement using two IR spotlights

In Experiment 4, the drone performed a 50 sec control task of traveling 15 m down an enclosed corridor and returning to the original position (Fig. 4) while using the two spotlights for feedback control.

## IV. RESULTS AND DISCUSSION

Figure 6 shows the distance measurement results of a comparison between the red fluorescent marker and different colored markers ( $100 \times 100$  (blue),  $150 \times 150$  (red),  $200 \times 200$  (green) mm) when the fixed camera (C270, Logicoool) was used during 15 m round trip movements in the corridor (Experiment 1 condition). The black line is the theoretical position determined by measuring from the two spotlight positions (Experiment 2 and 3 conditions). We found that the standard deviation (SD) of the estimated distance could be decreased by increasing the size of the red fluorescent marker. For example, in the timing of Period A (from 16 to 17 sec) of Fig. 6, the average and SD was as shown in Table 1. The real distance in Area A is approximately 10 m, and the estimated distances could be correctly measured by increasing the red marker area from  $100 \times 100$  to  $200 \times 200$  mm. Additionally, the SD could be decreased by increasing the red marker area. However, when the real distance increased to Area B (approximately 15 m, travel time from 20 to 25 sec), the estimation distances and SD began fluctuating and could not be stabilized because the red marker area appeared smaller than 10 dots in the camera view (Fig. 4b). As a result, the distance estimation process did not work well (Table 1). To estimate the distance by extracting the red marker area from the camera image, the marker area must be correctly measured in the image view, even when the marker area is small. In Experiment 1, as shown in Fig. 4a, the presence of numerous obstacles around the red marker position made it difficult to extract the red marker area.

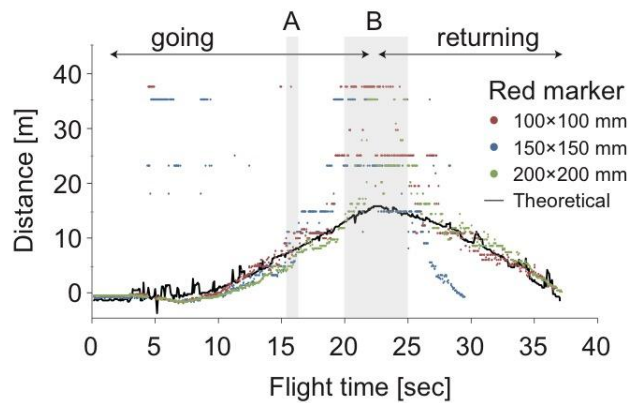


**FIGURE 6. Distance measurement results in the case of 15 m round trip movement in the case of a red fluorescent marker. Red markers of various sizes (100 × 100, 150 × 150, 200 × 200 mm) were attached at the rearward facing side of the drone.**

**TABLE 1**

**ESTIMATED DISTANCES AND FLUCTUATIONS FROM FLUORESCENT RED MARKER AREA A OR B IN FIG. 6**

Area A (10 m)	100×100 mm	150×150 mm	200×200 mm
Average [m]	16.0	15.4	11.9
S.D. [m]	2.26	0.69	0.47
Area B (15 m)	100×100 mm	150×150 mm	200×200 mm
Average [m]	26.1	36.0	31.9
S.D. [m]	8.68	10.99	9.29

Figure 7 shows the calculated distance results in cases when a single spotlight (red dots) and two spotlights (blue dots) were used during 15 m round trip movements. The vertical axis shows the calculated distance z [m] and the horizontal axis shows the flight time [sec]. The black line indicates the theoretical position of the drone as measured by the two spotlights positioned on the target side. In this experiment, the movement direction was changed at approximately 22 sec. The red dots (single spotlight) were difficult to calculate and unstable when the distance is approaching to 15 m when compared with the blue dots (two spotlights). In addition, z calculation errors of 18.6% were measured at odd intervals (area C) in the single spotlight (red dots) case. In the case of the two spotlights at the distance of 15 m, the SD was 0.31 m in the same area C. In addition, the distance S.D. at 15 m for a single spotlight was 10.6 m. Thus, it is clear that there were large distance measurement fluctuations in the single spotlights case. Table 2 shows Area C, which is the primary result of this study.

Based on the above experimental results, the two spotlights position measurement method works more effectively than the single spotlight method.

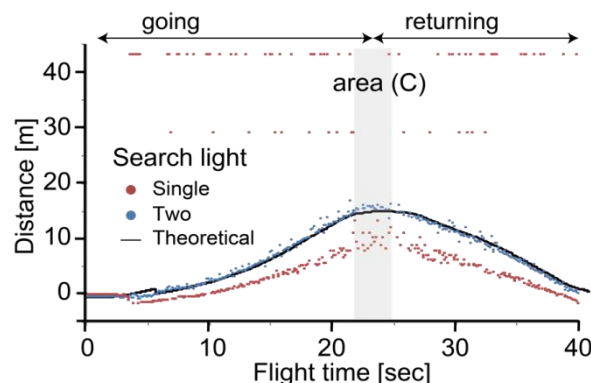


**FIGURE 7: Distance measurement during 15 m distance autonomous control experiment using both single and two spotlights in an enclosed corridor.**

**TABLE 2**  
**SINGLE AND TWO SPOTLIGHTS POSITION MEASUREMENT METHOD SHOWN IN FIG. 7**

Area C (15 m)	Single spotlight	Two spotlights
Average [m]	13.9	15.7
S.D. [m]	10.66	0.31

As for Experiment 4, Fig. 8 shows the 50 sec 15 m round trip results for an enclosed corridor (same experimental conditions as Fig. 5). The blue and red dots indicate the outbound and returning trajectories, respectively. The green area period's position average and SD calculations are shown on the left side of the figure. Based on these results, the average and SD of the 15 m round trip control were calculated as  $-0.13 (\pm 0.06)$  m (outbound) and  $0.09 (\pm 0.02)$  m (return).

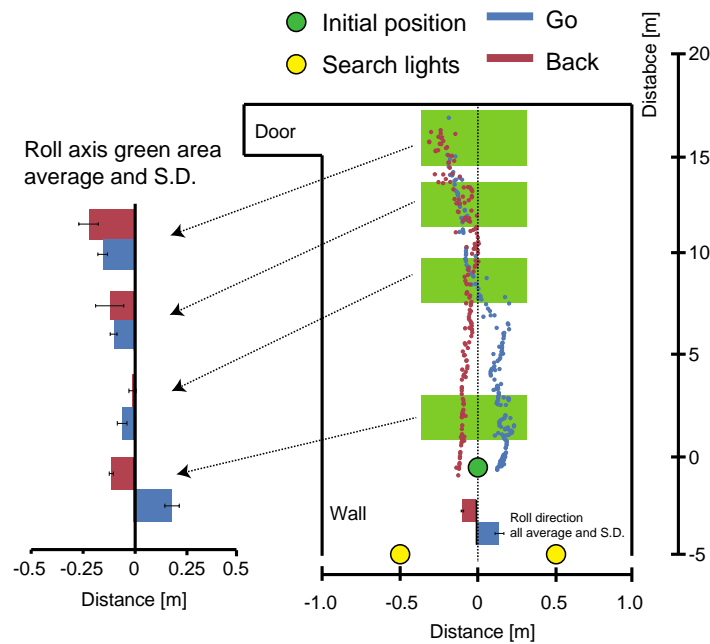


**FIGURE 8: 15 m distance autonomous control experiment using two spotlights in an enclosed corridor.**

As shown in the left bottom of Fig. 4a, even when the red marker size was large ( $200 \times 200$  mm) and the drone size was large (approximately  $500 \times 500 \times 50$  mm), the extracted red marker area at a distance of 15 m distance only measured from six to 10 dots in size. This appears to be the limit to the estimation distance when using a red marker attached to a drone moving straight ahead under constant floor lighting conditions in a university corridor. If the drone were to be moved outdoors, the distance estimation performance would deteriorate. In addition, we found that the large board red marker tended to destabilize the flight performance of the drone due to wind resistance, even when 10% forward or backward movement power was applied. One potential solution to the issue of reduced image size might be to use a higher resolution camera. However, the destabilization that results when attaching a large red marker board to the drone would still be unacceptable, especially in long distance inspections at sites such as bridges or tunnels.

One of the advantages of our proposed method is that the spotlight points are easy to find using bright IR regions. In addition, although misidentifications are possible if the sun is present in the camera image, positioning the spotlights on the ground makes it possible to use the accelerometer to ascertain the direction of gravity, and thus distinguish the spotlights from the sun.

## V. CONCLUSION

In this paper, a 10 m-range autonomous four-rotor helicopter (drone) movement control system that utilizes two high-power spotlights was proposed and autonomous flight test evaluations were performed. To realize drone flights in excess of 10 m under unstable GPS signal situations, such as under bridges or inside tunnels during periodic maintenance inspections, the ability of a drone to perform correct self-positioning measurements is indispensable for stable control. In our experiments, distance measurements were more stable when two spotlights were used in comparison to experiments conducted with a

single spotlight and those conducted with a red marker attached to the drone. And the 15-m-long distance measurement precision of the drone position shows an SD of 0.31 m. Our proposed method would be effective in situations where no skilled drone control operator is available and when flights requiring visual confirmation under adverse conditions are required.

### ACKNOWLEDGEMENTS

This work was supported by KouheiFujiuti, Shuichi Honda, Hiroaki Takano.

### REFERENCES

- [1] K. Nonami, F. Kendoul, S. Suzuki, W. Wang, D. Nakazawa, "Autonomous flying robots : unmanned aerial vehicles and micro aerial vehicles," Springer Japan. 2010.
- [2] Ministry of Land (Japan), Infrastructure and Transport, bridge maintenance Subcommittee, Liang maintenance technology site verification and evaluation of the results, March 19, 2015: Available from: <http://www.mlit.go.jp/common/001083014.pdf> (URL)
- [3] E. Altug, J. P. Ostrowski, C. J. Taylor, "Control of a quadrotor helicopter using dual camera visual feedback," *International Journal of Robotics Report*, vol.24, no.5, 2005, pp. 329-341.
- [4] B. Ludington, E. Johnson, G. Vachtsevanos, "Augmenting UAV autonomy: vision-based navigation and target tracking for unmanned aerial vehicles," *IEEE Robotics and Automation Magazine*, vol.13, no.3, 2006, pp. 63-71.
- [5] H. Takano, H. Toda, "Roll movement realized by yaw and roll command combination method of AR Drone 4 rotor helicopter for improving stability of automatic position stop," *International Conference on Advanced Mechatronics (ICAM 2015)*, Waseda University, Tokyo, Japan, Dec.5-8, 2015, pp. 53.
- [6] H. Toda, S. Honda, H. Takano, "Effectiveness of Fast Speed Yaw and Roll Control Switching Instead of Normal Roll Control for AR Drone 4 rotor Helicopter," *International Journal of Innovative Research in Advanced Engineering*, vol. 3, issue 7, JYAE10081, doi:10.17632/y52bmbgtkg.1., 2016.
- [7] H. Toda, H. Takano, "Effect of Discrete Yaw Direction Setting for 4 Roter Helicopter Control: Computer Simulation and AR. Drone Model Implementation," *International Journal of Innovative Research in Advanced Engineering*, vol. 3, issue 7, JYAE10086, doi:10.17632/cj8f3v6csr.1., 2016.
- [8] S. Honda, H. Toda, M. Kitani, G. Capi, "Development of small size 4 rotor helicopter automatic position control algorithm", 32nd Annual Conference of the Robotics Society of Japan, 1D3-01, 2013.
- [9] S. Honda, H. Toda, M. Kitani, G. Capi, "Development of 4 rotor automatic flight control system using image processing filters that can be self-position estimation in natural objects with the aim of the reactor building spot," *ROBOMECH 2014*, March, Toyama, 2014.
- [10] S. Azrad, F. Kendoul, K. Nonami, "Visual Servoing of Quadrotor Micro-Air Vehicle Using Color-Based Tracking Algorithm," *Journal of System Design and Dynamics (JSME)*, vol. 4, no. 2, 2010, pp. 255-268.
- [11] B. Ludington, E. Johnson, G. Vachtsevanos, "Augmenting UAV autonomy: vision-based navigation and target tracking for unmanned aerial vehicles," *IEEE Robotics and Automation Magazine*, vol. 13, no. 3, 2006, pp. 63-71.
- [12] K. Nonami, "Rotary Wing Aerial Robotics," *Journal of Robotics Society of Japan*, vol. 24(8), 2006-11-15, pp. 890-896.
- [13] J. Engel, J. Sturm, D. Cremers, "Camera-based navigation of a low-cost quadcopter," *Intelligent Robots and Systems (IROS)*, 2012.
- [14] R. Mahony, T. Hamel, "Image-based visual servo control of aerial robotic systems using linear image features," *IEEE Trans. on Robotics*, vol.21, no.2, 2005, pp. 227-239.
- [15] Y. Kubota, T. Iwatani, "Dependable visual servoing of a small-scale helicopter with a wireless camera," *15th International Conference on Advanced Robotics (ICAR)*, 20-23 June 2011.
- [16] T. K. Roy, M. Garratt, H. R. Pota, M. K. Samal, "Robust altitude control for a small helicopter by considering the ground effect compensation," *10th World Congress of Intelligent Control and Automation (WCICA)*, DOI:10.1109/WCICA.2012.6358168, 2012, pp. 1796-1800.
- [17] O. Andrisani, E. T. Kim, J. Schierman, F. P. Kuhl, "A nonlinear helicopter tracker using attitude measurements," *IEEE Transactions on Aerospace and Electronic Systems*. vol.27, issue: 1, DOI:10.1109/7.68146, 1991, pp. 40-47.
- [18] F. Chen, B. Jiang, F. Lu, "Direct adaptive control of a four-rotor helicopter using disturbance observer," *International Joint Conference on Neural Networks (IJCNN)*, 2014, pp. 3821-3825.
- [19] A. C. Satici, H. Poonawala, M. W. Spong, "Robust Optimal Control of Quadrotor UAVs," *IEEE Access*. 2013, vol. 1, DOI:10.1109/ACCESS.2013.2260794, 2013, pp. 79-93.
- [20] J. Toledo, L. Acosta, M. Sigut, J. Felipe, "Stability Analisis of a Four Rotor Helicopter," *Automation Congress 2006, WAC '06. World*, 2—6, pp. 1-6.
- [21] P. Castillo, A. Dzul, R. Lozano, "Real-time stabilization and tracking of a four-rotor mini rotorcraft," *IEEE Transactions on Control Systems Technology*, vol. 12, issue: 4, DOI:10.1109/TCST.2004.825052, 2004, pp. 510-516.
- [22] O. Meister, N. Frietsch, C. Ascher, G. F. Trommer, "Adaptive path planning for a VTOL-UAV," *Position, Location and Navigation Symposium, 2008 IEEE/ION*, DOI:10.1109/PLANS.2008.4570046, 2008, pp. 1252-1259.
- [23] L. Garcia-Delgado, A. Dzul, V. Santib, M. Llama, "Quad-rotors formation based on potential functions with obstacle avoidance," *Control Theory and Applications, IET*, vol. 6, issue:12, DOI:10.1049/iet-cta.2011.0370, 2012, pp. 1787-1802.

- 
- [24] F. Kendoul, Z. Yu, K. Nonami, "Embedded autopilot for accurate waypoint navigation and trajectory tracking: Application to miniature rotorcraft UAVs," IEEE International Conference on Robotics and Automation, 2009. ICRA '09, DOI:10.1109/ROBOT.2009.5152549, 2009, pp. 2884-2890.
- [25] K. Nomura, "Industrial applications type electric multi-rotor helicopter," introduction of mini-surveyor and flight demonstration. Mini-surveyor consortium: Available from <http://mec2.tm.chiba-u.jp/~nonami/consortium/outline.html/> (url)
- [26] E. Altu, J. P. Ostrowski, R. Mahony, "Control of a Quadrotor Helicopter Using Visual Feedback," Proceedings of the 2002 IEEE International Conference on Robotics and Automation, Washington DC, May 2002.
- [27] Y. Yoshihara, K. Watanabe, T. Iwatani, K. Hashimoto, "Image-based visual servo control for a micro helicopter under partial occlusions," Proceedings of 2007 JSME Conference on Robotics and Mechatronics, ID 2A2-A06, Akita, Japan, May 10-12, 2007.
- [28] K. Watanabe, Y. Iwatani, N. Kenichiro, K. Hashimoto, "A vision-based support system for micro helicopter control," Proceedings of the 2008 Conference on Robotics and Mechatronics, ID 1P1-F13, Nagano, Japan, June 5-7, 2008.
- [29] Y. Kubota, T. Iwatani, "Dependable visual servoing of a small-scale helicopter with a wireless camera," Proceedings of the 2008 Conference on Robotics and Mechatronics. ID 1A2-O15, Okayama, Japan, May 26-28, 2011.
- [30] S. Yoshida, Engineeringnavi. library of ARDroneForP5: Available from <http://kougaku-navi.net/ARDroneForP5/> (URL).

# Parametric Analysis of Interlaminar Toughness of Unidirectional Carbon Fiber and Woven Carbon Fabric Composites

Panagiotis J. Charitidis

Department of Environmental Engineer, Democritus University of Thrace, Xanthi-Greece

**Abstract**—The present study focusses on the parametrical investigation of unidirectional and woven carbon fiber double cantilever beams subjected to mode I, in order to study its effects on their strength and failure. Different crack lengths as well as width and thickness of the specimens have been analyzed extensively. The maximum normal and shear stresses are found to decrease as the crack length increases for both types of composites. The crack length directly affects the strength of the specimens. A numerical model was developed using the Comsol Multiphysics to predict the failure of double cantilever beams. The crack initiation and progression in the specimens was predicted using the cohesive zone method (CZM) and the delamination at the interface.

**Keywords**—fracture toughness, uni-directional, woven fabric, crack propagation, double cantilever beam.

## I. INTRODUCTION

The literature review shows that carbon fiber reinforced composites have been widely used in a variety of structural applications in the aerospace, automotive and civil industry [1-19]. High specific modulus (stiffness to weight ratio) and intralaminar tensile fracture toughness [20] are possible the main reasons in the widespread use of these composites. Moreover, the intralaminar tensile fracture toughness is relevant not only to material qualification for the design of composite aerostructures, but also to the definition of the softening laws used in the computational models for predicting the behavior of composite structures [20]. Laminated composite materials made of brittle matrices are susceptible to interlaminar cracks (interlaminar mode of fracture -delamination) and to propagation of that cracks also. Especially low-velocity impact damage and micro-cracks formed during manufacturing, service, or maintenance cause to delamination in laminated composite materials. It is interesting to note that, the performance evaluation of the advanced reinforcing fibers such as carbon [21,22], and epoxy resins [23-26], in final composite is necessary for their safe application, especially for the manufacturing of large light weight structures[3, 5-7].

For the composites of interest, the delamination process is typically brittle. Cracks in the form of delaminations and disbonds are the most common failure modes observed in composite structures [27]. One approach to solve this problem involves the use of three-dimensional woven and braided reinforcements [28-32]. Fiber stitching [33] or architected adhesives [34] are also alternative methods for solving such problems. It should be mentioned that interlaminar fracture resistance [35, 36] remains a weakness of polymer composites. Such property indicates the amount of stress required to propagate a pre-existing thin crack. On the other hand, damage tolerance is the desired basic property for various structures depending upon the end application [37]. A more systematic and theoretical analysis is required for fracture toughness characterization of composites which is still on the way of growth as compared to metals.

Several theories have been proposed to composites, some focusing on the fracture toughness associated with fibre-dominated tensile failure [38-42], others on the fracture characteristics of composite laminates and developed a fracture criterion which showed that the critical stress intensity factor for fibre failure is a material constant [43], as well as the tensile intralaminar fracture toughness of woven composite laminates [44]. Woven fiber reinforcement is typically used in applications where multidirectional laminates are required (ship hull). It should be mentioned that woven fabric composites exhibit relatively unstable crack growth compared to unidirectional laminates [45, 46]. Unstable crack growth in woven fabric composites can be observed as the crack jumps between transverse tows. Woven fabrics tend to have heavier tows (e.g., higher filament count) than unidirectional reinforcement. Another parameter that affects the fracture toughness is the width of the specimen which does not affect the fracture toughness of unidirectional composites [47]. Moreover, for the case of woven composites, further investigation is needed to determine size effects of woven fabric composites on fracture toughness.

Unidirectional composites and woven fabric composites are physically different in that the individual fibers are bonded in unidirectional composites, whereas fiber bundles or tows are bonded in woven fabric composites. For a heavy woven fabric composite, the number of tows per specimen width will depend on where the specimen is cut from a panel, which can result in an increase in variability. Several existing studies in the broader literature have examined the variability of fracture

toughness in woven fabric composites [48, 49]. Toughening mechanisms in heavy woven fabric composites vary from the mechanisms exhibited in unidirectional laminates. Unidirectional laminates undergo significant fiber bridging when subjected to mode I fracture; [50] however, the weave in woven fabric composites limits the amount of fiber bridging which can occur [45]. Other toughening mechanisms include the presence of inclusions and resin-rich areas. Energy can be stored behind a transverse tow as it acts like an inclusion within the laminate, causing the crack to deviate from the mid-plane of the fracture specimen. The amount of energy capable of being stored behind each tow is highly variable due to thickness variations in the woven fabric. Additionally, it is possible for resin-rich areas to form in a regular pattern as a result of the weave structure. The result is unstable crack propagation for woven fabric composites made with heavy woven fabrics. Research has shown that both the thickness and location of the end of the film used to create the initial crack within the laminate can affect the observed fracture toughness at onset [51, 52].

It is well known, that the critical strain energy release rate (SERR) occurs immediately before crack growth and is commonly defined as  $G_c$ . Fracture toughness of laminated composite materials under static loading has been shown to be dependent on the relative amounts of  $G_I$  and  $G_{II}$  [53]. Mixity is typically used to describe what portion of the total SERR comes from  $G_I$  and  $G_{II}$  and is defined as the ratio of  $G_{II}$  to  $G_T$ . The  $G_c$  value at which the delamination essentially starts to spread differs largely depending on the mode of loading [16]. As the material is being tested and the crack begins to propagate, the stiffness and force on the material begin to decrease. The decrease in the load means that the strain energy stored in the material is also reducing or being released.

Finite element method has become the most popular numerical method for delamination modelling. Virtual Crack Closure Technique (VCCT) and Cohesive Zone Method (CZM) are mainly used to predict delamination growth. These techniques have potential to solve contemporary problems in components of the strain energy release rate. In comparison with other techniques; VCCT has the advantage of analyzing crack propagations in laminated composite materials with brittle matrix. The literature review shows that VCCT can be used to characterize of mode I delamination growth [54, 55]. Some authors [56] have also suggested that VCCT can be used to simulate mode I delamination growth even though the technique exhibits significantly overestimated critical strain energy release rate. Moreover, Bonhomme et al. [57] investigated mode I interlaminar fracture toughness of carbon/epoxy composite by using a two-step numerical method similar to the VCCT.

The use of cohesive zone method was introduced by Barenblatt [58] and Dugdale [59]. A difference between these methods can be attributable to the nature of materials (brittle and ductile). Barenblatt method removes stress singularity at the crack tip (in atomic scale), while Dugdale introduce the concept that stresses in the material are confined by the yield stress. That means, a plastic zone is generated in front of the crack tip. This method as well as VCCT can be used in 2D and 3D problems [60, 61]. The most difficult part for this method is the size of the FE mesh, which increases the time and the cost of the analysis. Furthermore, it suffers from convergence problems. In order to reduce the cost, is to use beam finite element elements instead of plane solids to model the bulk material of the specimens in 2D analysis of delamination [62, 63], but it will suffer from convergence problems and spurious oscillations. A cohesive zone model is frequently used in various types of materials and applications [64, 65, 66], but the traction-separation law must be defined (shape, cohesive strength, and fracture toughness).

A large number of existing studies in the broader literature have examined models such as traction-separation based on an exponential form, a trapezoidal form and the bilinear form [65]. The most difficult part is the direct measurement of these parameters by the experimental procedure. This is the reason that numerical analysis was based on an idealized cohesive zone model [64, 67, 68]. For instance, Turon [68] used bilinear cohesive zone model to estimate these parameters, while the effects of the cohesive law on ductile crack propagation was investigated by Yuan and Li [69].

The aim of this research is to investigate parametrically the effects of crack length on the double cantilever beam while the width and thickness of the sub laminates varies.

## II. MATERIALS AND METHODS

### 2.1 Joint Configuration and Materials

The “testing” configuration was based on the ASTM standards D5528-13 for Mode I Interlaminar Fracture Toughness of Unidirectional Fiber-Reinforced Polymer Matrix Composites. It is well known double cantilever beam is the most widely used test configuration for the study of crack propagation and arrest for composite materials and adhesives. In this context, in order to investigate the influence of crack length on the DCB specimen, four different crack lengths ( $a_0$ ) were used: 10, 20, 30 and 40mm. The lever length was kept constant at 44.5mm for all the configurations while the specimen’s width (W) was

varied from 20mm to 25mm. Similarly, the thickness ( $t$ ) of the two sub-laminates also varied from 1.5mm to 1.75mm, respectively (figure 1). Moreover, two different types of composites were adopted in the present parametrical procedure. Firstly, the unidirectional carbon epoxy composite and secondly the woven carbon epoxy composite, where the mechanical properties are shown in table 1.

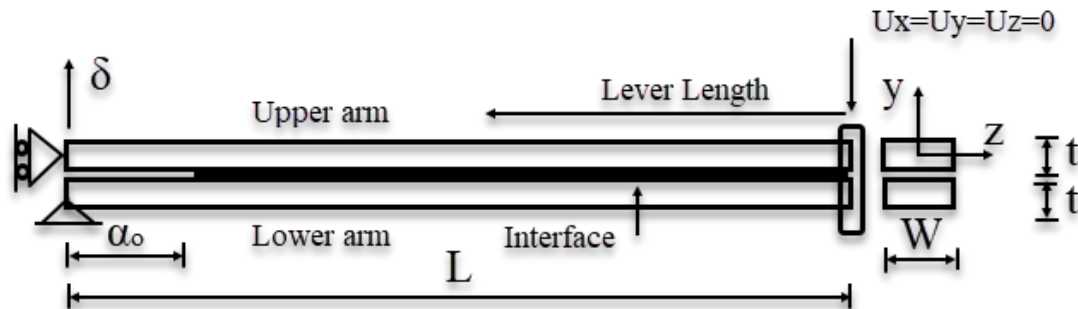


FIGURE 1: A test specimen configuration.

TABLE 1

MATERIALS PROPERTIES FOR (A) UNIDIRECTIONAL CARBON FIBER, (B) WOVEN CARBON FIBER COMPOSITES.

Property	Unidirectional CF/Epoxy	Woven CF/Epoxy
$\{\rho, \text{kg/m}^3\}$	$\{1570\}$	$\{1570\}$
$\{E_1, E_2, E_3, \text{GPa}\}$	$\{122.7, 10.1, 10.1\}$	$\{59.5, 7.46, 7.46\}$
$\{v_{12}, v_{23}, v_{13}\}$	$\{0.25, 0.45, 0.25\}$	$\{0.035, 0.31, 0.035\}$
$\{G_1, G_2, G_3, \text{GPa}\}$	$\{5.5, 3.7, 5.5\}$	$\{5.18, 5.18, 5.18\}$
$\{G_I, G_{II}, \text{kJ/m}^2\}$	$\{0.969, 1.719\}$	$\{0.252, 0.665\}$
{Benzeggagh-Kenane}	$\{2.84\}$	$\{2.89\}$

### III. FINITE ELEMENT METHOD

#### 3.1 Model Parameters and Loading

The numerical analyses were performed in the Comsol Multiphysics software based on the boundary finite element. To reflect the real behavior of DCB samples during numerical tests on lines (3D) corresponding to the piano hinge locations, the boundary conditions were assumed. In our case, the boundary conditions are shown in figure 1. The displacement was constant at 0.006m, which held constant for all cases. The size of the element was 1/10, in order to reduce the computation time as well as the oscillations [70]. The minimum increment time step allowing to achieve satisfactory results has been set at 0.001 which is a value about ten times higher than the value assumed in [71].

The interfacial failure in the specimens was simulated by using the cohesive zone method, where the behavior is described in terms of a traction-separation equation (figure 2). According to figure 2, the cohesive zone method is based upon the assumption that cohesive bonding exists between two separated surfaces and progressive events of failure (along 0A-AC) are governed by a reduction of stiffness of interface between the two surfaces [72, 73]. The complete fracture obtains at point C ( $D_i=1$ ).

Furthermore, it is assumed that the penalty stiffness ( $K_{nn}$ ,  $K_{ss}$  and  $K_{tt}$ ) was kept constant for all modes ( $10^6 \text{ N/mm}^3$ ) [70]. By keeping the penalty stiffness equal to  $10^6 \text{ N/mm}^3$ , the overall stiffness of the specimen is not affected by the applied displacement. A linear degradation was used for the damage evolution in which the Benzeggagh-Kenane (BK) fracture criterion [73, 74] was employed to define the mix mode softening of the cohesive surface, while a quadratic stress criterion was considered ( $t_n$ ,  $t_s$  and  $t_t$  are the interface strength). It should be noted that  $t_n$  must be positive (intension) to initiate the delamination at the interface. The normal strength and the shear strength for unidirectional and woven carbon/epoxy composites are  $\{80\text{MPa}, 30\text{MPa}\}$  and  $\{100\text{MPa}, 60\text{MPa}\}$ , respectively.

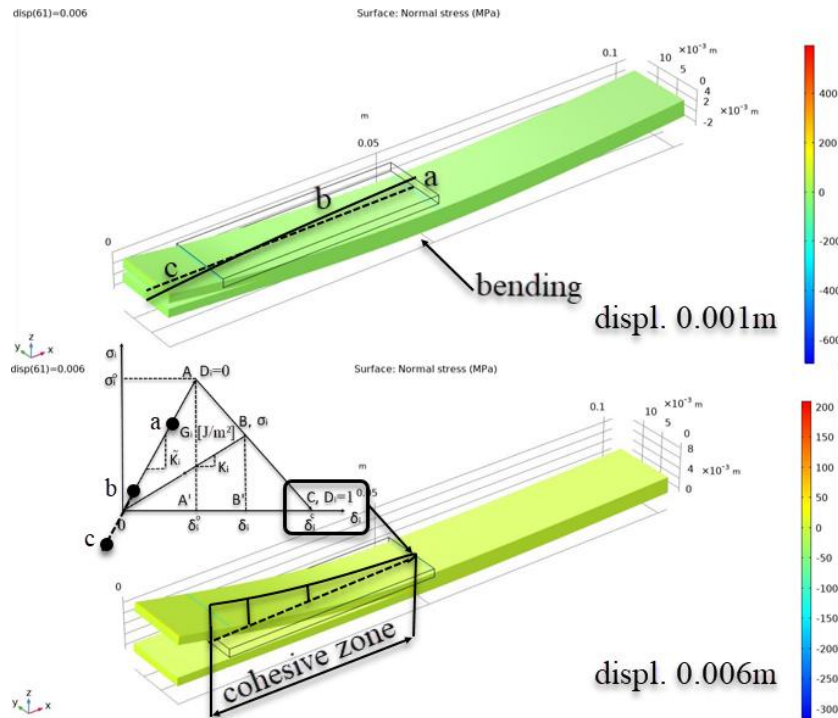
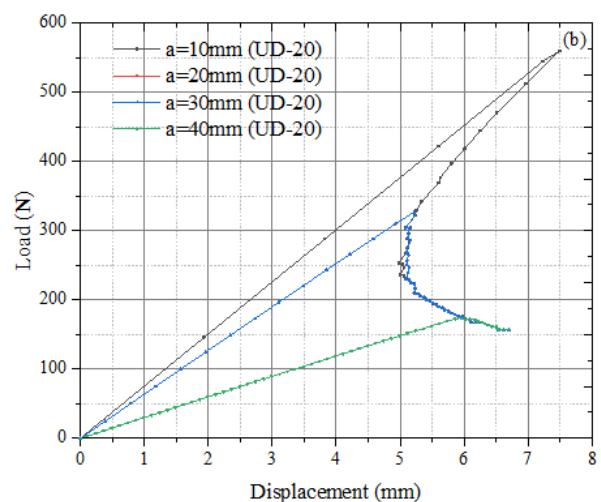
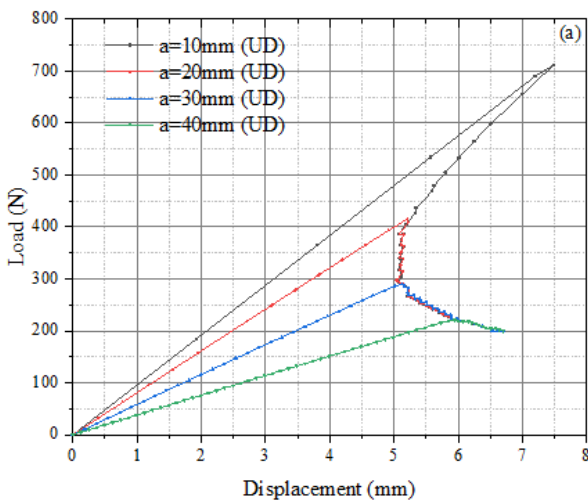


**FIGURE 2: Traction-separation law**

**IV. RESULTS AND DISCUSSION**

Fig. 2 a-d and 3 a-d presents the load-displacement curves for unidirectional carbon/epoxy and woven carbon epoxy composite specimens for different crack lengths, width, and thickness of the sub laminates. A significant effect of the crack length can be observed, independently to the type of the material. Crack initiation appears where the first change of the slope in the diagrams is visible. The load-displacement curve shows that the load increases up to a certain point. After that point, it gradually decreases for both cases. To be more specific, in the case of unidirectional composites an average 69.5% decrease of the load can be observed when increasing the crack length from 10 to 40 mm. For the case of the woven composites is almost 70.5%. The value of displacement is chosen in a way that the specimens remains elastic everywhere.

However, the effect of geometric nonlinearity on the mode I fracture toughness of composite materials is suffice for long cracks [75, 76]. However, according to Figures 2a-d, there must be a limit of the crack length in double cantilever beams, especially for unidirectional composites. In other words, it is more benefit to manufacture specimens with crack length up to 20mm (figure 2d and d). Such limits must be defined by the selection of the appropriate normal and shear strength behavior and the geometry of the specimen. Further on, to avoid the sawing teeth in load-displacement curves, a finer mesh should be employed.



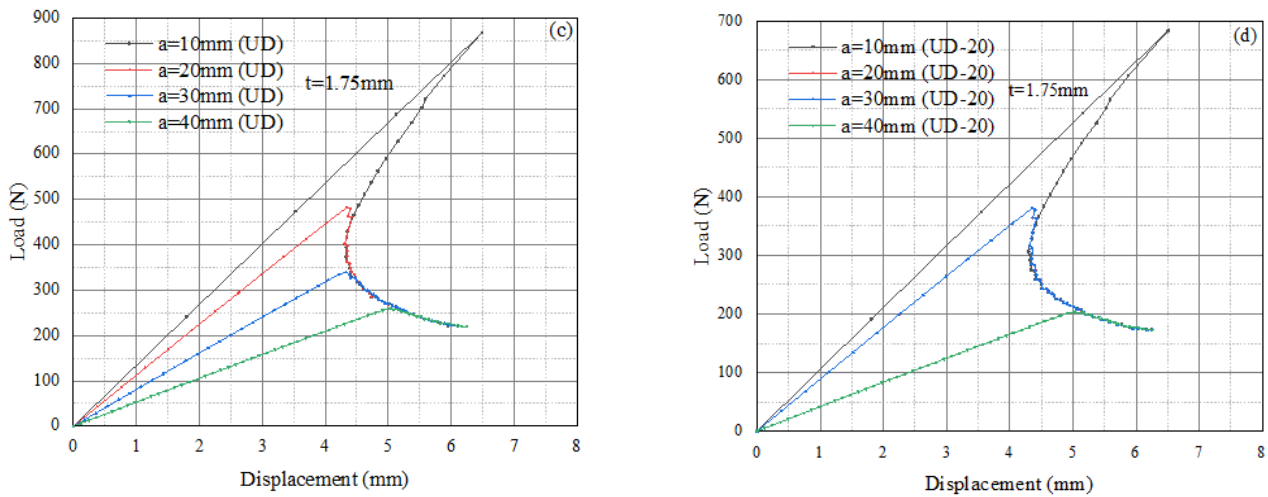


**FIGURE 3: Load - Displacement curves for unidirectional carbon epoxy composites with different crack lengths of model with : case a)  $t=1.5\text{mm}$  and  $w=25\text{mm}$ , case b)  $t=1.5\text{mm}$  and  $w=20\text{mm}$ , case c)  $t=1.75\text{mm}$  and  $w=25\text{mm}$ , and case d)  $t=1.75\text{mm}$  and  $w=20\text{mm}$ .**

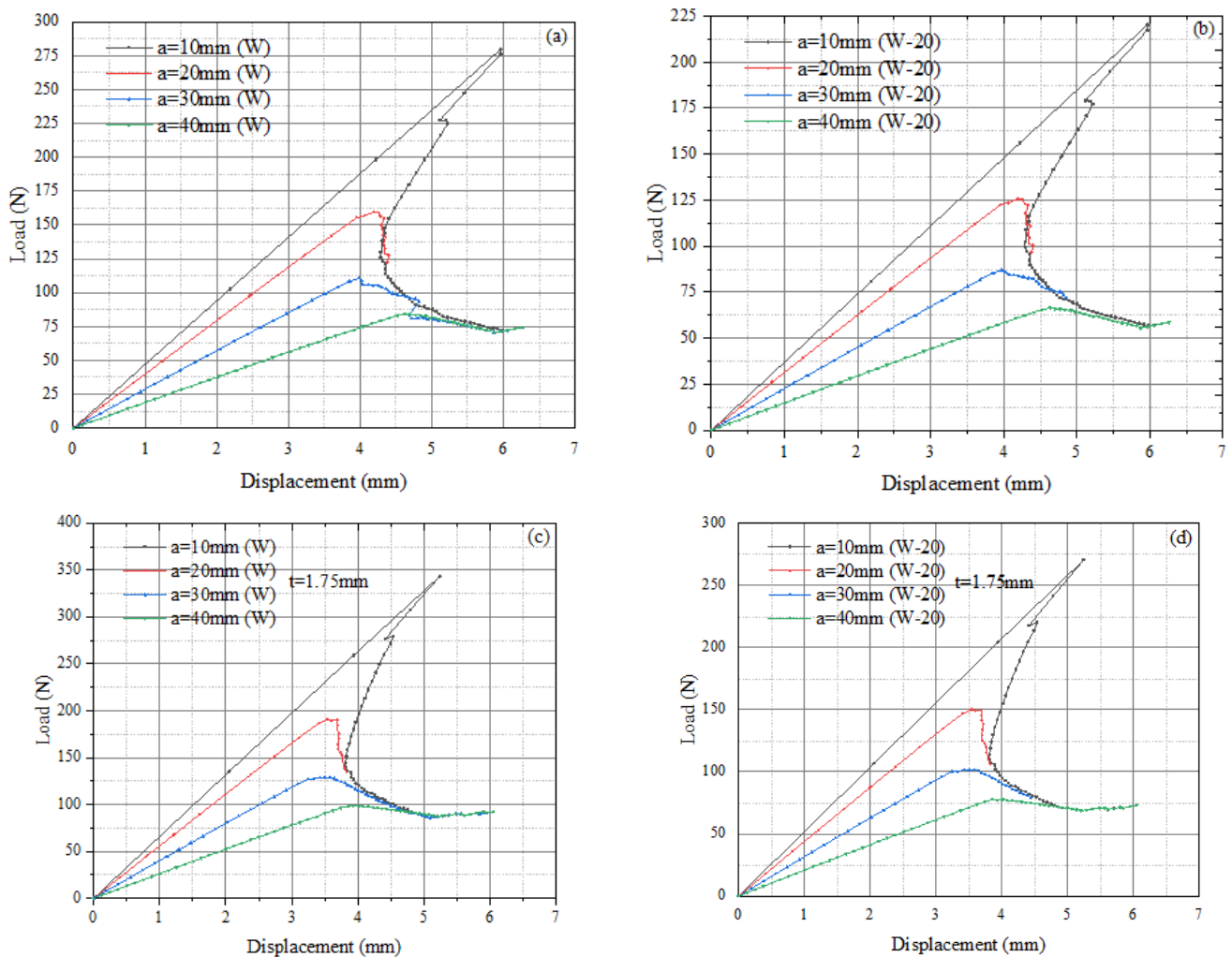


**FIGURE 4: Load - Displacement curves for unidirectional carbon epoxy composites with different crack lengths of model with : case a)  $t=1.5\text{mm}$  and  $w=25\text{mm}$ , case b)  $t=1.5\text{mm}$  and  $w=20\text{mm}$ , case c)  $t=1.75\text{mm}$  and  $w=25\text{mm}$ , and case d)  $t=1.75\text{mm}$  and  $w=20\text{mm}$ .**

As one increases the crack length, the averaged normal stress between these two types of materials is decreased by 59.29% for the cases a and b, and 99.30% for the cases c and d, respectively (averaged). On the other hand, the averaged shear stress is further reduced at the surface of the sub-laminate, by 38.02% for the cases a and b, and 99.93% for the cases c and d, respectively (table 2).

**TABLE 2**  
**UNIDIRECTIONAL CARBON/EPOXY AND WOVEN CARBON/EPOXY COMPOSITES RESULTS: NORMAL STRESS AND SHEAR STRESS [MPa].**

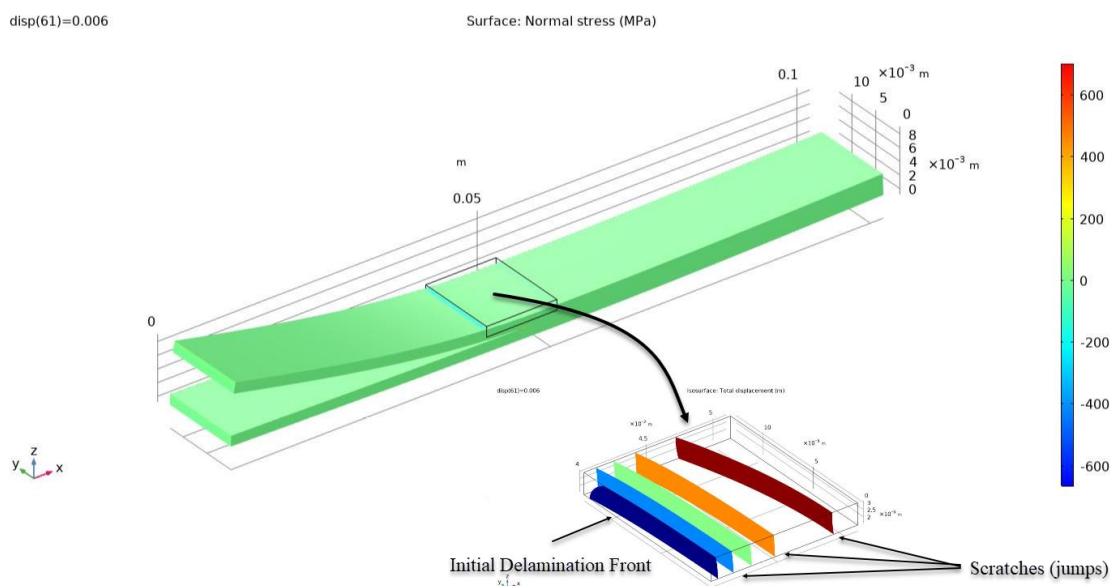
Crack Length	10 mm		20 mm		30 mm		40 mm	
Normal Stress	UD	W	UD	W	UD	W	UD	W
a	52.88	21.34	52.85	21.52	52.82	21.63	53.36	21.22
b	52.80	21.58	52.79	21.70	52.79	21.89	52.95	21.41
c	46.30	0.32	46.30	0.33	46.29	0.33	46.31	0.33
d	46.36	0.32	46.36	0.33	46.36	0.32	46.37	0.32

Crack Length	10mm		20mm		30mm		40mm	
Shear Stress	UD	W	UD	W	UD	W	UD	W
a	68.83	42.37	68.87	42.52	68.72	42.61	68.99	42.28
b	68.38	42.59	68.38	42.69	68.38	42.84	68.52	42.45
c	66.10	6.64	66.10	6.69	66.07	6.64	66.16	6.67
d	66.43	6.68	66.41	6.74	66.41	6.65	66.50	6.64

The results show that unidirectional laminates undergo significant fiber bridging when subjected to mode I fracture; [50] however, the weave in woven fabric composites limits the amount of fiber bridging which can occur [45]. The width of the specimens is another parameter that affects the fracture toughness of woven composites, but not for unidirectional composites [47]. Moreover, woven fabric composites exhibit relatively unstable crack growth compared to unidirectional laminates [45, 46].

Unstable crack growth in woven fabric composites can be observed as the crack scratches or jumps between transverse tows (fig. 5). Scratches means, load drops at the interface, which will be decreased or disappear due to the presence of the fiber bridging phenomenon [77]. Based on the traction-separation law, a new crack is formed once the critical force value is exceeded. This also means that subsequently a new critical force (but lower) must be surpassed again at the time of next crack propagation. It is hence necessary to accurately capture such progress of failure in a smooth manner. The bending of sub-laminates drastically changes both the normal stress and shear stress concentrations at the interface (fig. 2 and 6).



**FIGURE 5: Scratches (jumps) on the surface of the sub-laminate.**

According to figure 6, on the length of the interface area exists where composites is under compression for all unidirectional carbon epoxy. But not for the case of woven composites. A comparative study of normal and shear stress variations for different crack lengths is made; it can be observed that, as the crack length increases, the maximum shear strength decrease in interface (table 2). Taking into account all these, the area where the normal stresses (tensile) appear is always confined almost to the ends of the cohesive zone. It exceeds typically 0.005m from the edge of the lever length for different crack lengths. This means that normal stresses are much more localized and are introduced mainly by the rotation and bending of the sublaminates. However, for woven composites (figure 7) shows that the maximum normal and shear stresses appears at the lever length. This difference is may be due to the amount of bridging, or to the amount of energy capable of being stored in the specimen.

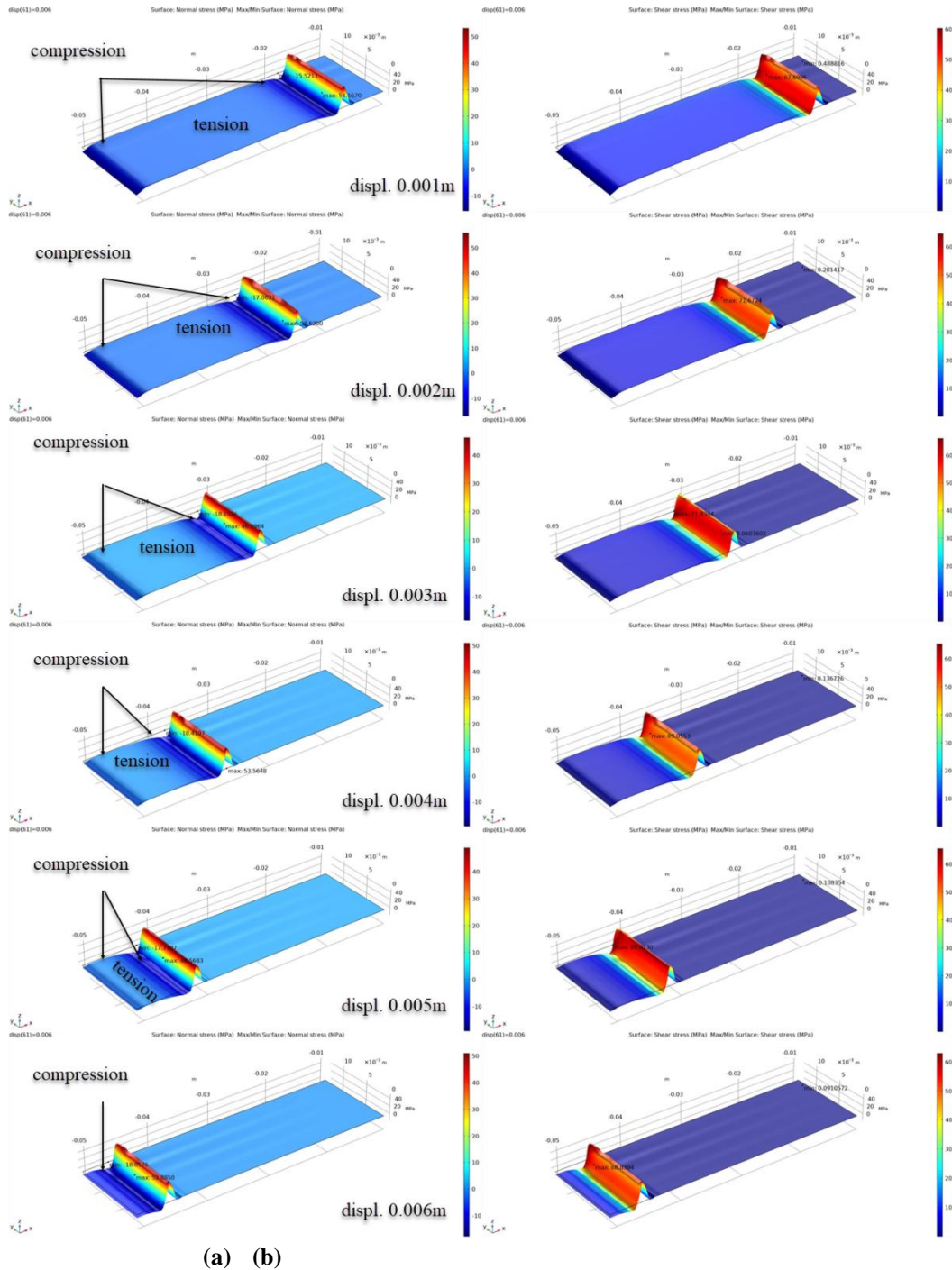


**FIGURE 6: Normal (a) and shear (b) stress distribution at the interface, crack length of 10mm (unidirectional carbon/epoxy, case a) [MPa].**

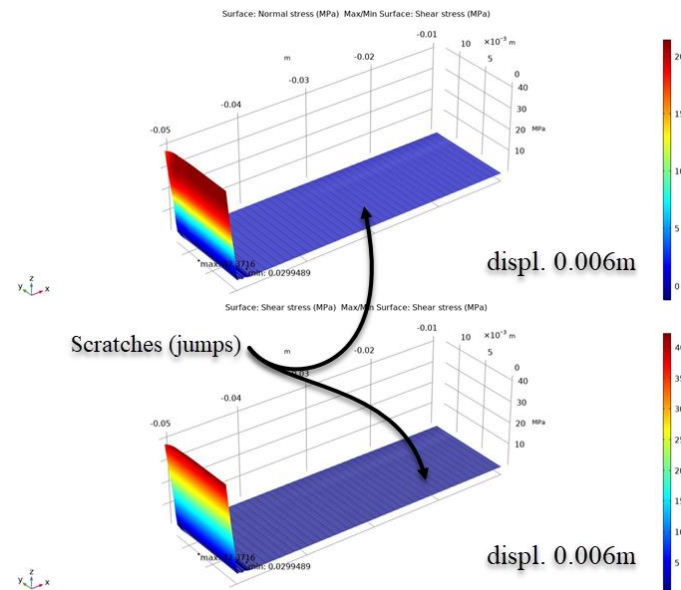


**FIGURE 7: Normal (a) and shear (b) stress distribution at the interface, crack length of 10mm (woven carbon/epoxy, case a) [MPa].**

## V. CONCLUSION

As already mentioned, double cantilever beam is the most widely used test configuration for the study of crack propagation and arrest for composite materials. In this study, the following conclusions can be made,

- The durability of the double cantilever beam is affected by the sub-laminate surface quality and the service loads.
- There must be a limit of the crack length in double cantilever beams, especially for unidirectional composites.
- To avoid the sawing teeth in load-displacement curves, a finer mesh should be employed.
- The width of the specimens affects the fracture toughness of woven composites, but not for unidirectional composites.
- Unstable crack growth in woven fabric composites can be observed as the crack scratches or jumps between transverse tows.
- The bending of sub-laminates drastically changes both the normal stress and shear stress concentrations at the interface.

## REFERENCES

- [1] B.G.Falzon, "Impact damage and repair of composite structures", Aeronautical J, vol. 113, pp. 431-445, 2009.
- [2] D. H. J. A.Lukaszewicz, "Automotive composite structures for crashworthiness in: El-marakbi A, Advanced composite materials for automotive applications: Struct.Integ. and Crashw., Wiley, 2013, pp. 100-127.
- [3] S. Rana and R. Figueiro, Advanced composites materials for aerospace engineering, Woodhead Publishing, United Kindom, 2016.
- [4] D. Song and R. K. Gupta, "The use of thermosets in the building and construction industry in: Guo QP" Thermosets: Structure, Properties, and Applications, Elsevier, 2012, pp. 165-188.
- [5] H. D. Stenzenberger, "Recent developments of thermosetting polymers for advanced composites," Compos. Struct., vol. 24, pp. 219-231, 1993.
- [6] R. Pascault and J. J. Williams, "Overview of thermosets: Present and future in: Guo QP", Thermosets: Structure, Properties, and Applications, Elsevier, 2018, pp. 3-34.
- [7] J. Takahashi and Y. Wan, "Tensile and compressive properties of chopped carbon fiber tapes reinforced thermoplastics with different fiber lengths and molding pressures," Compos. Part A, vol. 87, pp. 271-281, 2016.
- [8] L. G. Blok, M. L. Longana, H. Yu, B. K. S. Woods, "An investigation into 3D printing of fibre reinforced thermoplastic composites," Addit.Manuf, vol. 22, pp. 176-186, 2018.
- [9] S. S. Yao, F. L. Jin, K. Y. Rhee, D. Hui and S. J. Park, "Recent advances in carbon-fiber-reinforced thermoplastic composites: A review," Compos. Part B, vol.142, pp. 241-250, 2018.

- [10] M. Biron, "Future prospects for thermoplastics and thermoplastic composites in: Biron M," *Thermopl. and Thermopl. Compos. Plast. Des. Lib.*, 2018, pp. 1083-126.
- [11] C. Ceccato, M. Salviato, C. Pellegrino and G. Cusatis, "Simulation of concrete failure and fiber reinforced polymer fracture in confined columns with different cross-sectional shape," *Int. J. Solids Struct.*, vol. 108, pp. 216-29, 2017.
- [12] A. Couture, J. Laliberte and C. Li, "Mode I fracture toughness of aerospace polymer composites exposed to fresh and salt water," *Chem. Mater. Eng.*, vol. 1, pp. 8-17, 2013.
- [13] O. Do" brich, T. Gereke and C. Cherif, "Modeling the mechanical properties of textile reinforced composites with a near micro-scale approach," *Compos. Struct.*, vol. 135, pp. 1-7, 2016.
- [14] A. Elias, F. Laurin and M. Kaminski, "Experimental and numerical investigations of low energy/velocity impact damage generated in 3D woven composite with polymer matrix," *Compos. Struct.*, vol. 159, pp. 228-239, 2017.
- [15] W. X. Wang, Y. Takao and T. Matsubara, "Improvement of the interlaminar fracture toughness of composite laminates by whisker reinforced interlamination," *Compos. Sci. Tech.*, vol. 62, pp. 767-774, 2002.
- [16] Y. Tanzawa, N. Watanabe and T. Ishikawa, "FEM simulation of a modified DCB test for 3-D orthogonal interlocked fabric composites," *Compos. Sci. Tech.*, vol. 61, pp. 1097-1107, 2001.
- [17] Y. Iwahori, K. Nakane and N. Watanabe, "DCB test simulation of stitched CFRP laminates using interlaminar tension test results," *Compos. Sci. Tech.*, vol. 69, pp. 2315-2322, 2009.
- [18] P. Coronado, A. Arguelles and J. Vina, "Influence of low temperatures on the phenomenon of delamination of mode I fracture in carbon-fibre/epoxy composites under fatigue loading," *Compos. Struct.*, vol. 112, pp. 188-193, 2014.
- [19] E. Borowski, E. Soliman and U. Kandil, "Interlaminar fracture toughness of CFRP laminates incorporating multi-walled carbon nanotubes," *Polymers*, vol. 7, pp. 1020-1045, 2015.
- [20] G. Catalanotti, J. Xavier and P. P. Camanho, "Measurement of the compressive crack resistance curve of composites using the size effect law," *Composites Part A: Appl. Sci. and Man.*, vol. 56, pp. 300-307, 2014.
- [21] H. Zhao, L. Chen and J. Yun, "Improved thermal stabilities, ablation and mechanical properties for carbon fibers/phenolic resins laminated composites modified by silicon containing polyborazine," *Eng. Sci.*, vol. 2, pp. 57-66, 2018.
- [22] A. Siddique, B. Sun and B. Gu, "Structural influences of two-dimensional and three-dimensional carbon/epoxy composites on mode I fracture toughness behaviors with rate effects on damage evolution," *J. Ind. Text.*, pp. 1-23, 2018 <https://doi.org/10.1177/1528083718819871>.
- [23] Y. Huangfu, C. Liang, and Y. Han, "Fabrication and investigation on the Fe<sub>3</sub>O<sub>4</sub>/thermally annealed graphene aerogel/epoxy electromagnetic interference shielding nanocomposites," *Compos. Sci. Tech.*, vol. 169, pp. 70-75, 2019.
- [24] C. Liang, H. Qiu and Y. Han, "Superior electromagnetic interference shielding 3D graphene nanoplatelets/reduced graphene oxide foam/epoxy nanocomposites with high thermal conductivity," *J Mater Chem C* 2019; 7: 2725-2733.
- [25] J. Gu, C. Liang and X. Zhao, "Highly thermally conductive flame-retardant epoxy nanocomposites with reduced ignitability and excellent electrical conductivities," *Compos. Sci. Tech.*, vol. 139, pp. 83-89, 2017.
- [26] Y. Huangfu, K. Ruan and H. Qiu, "Fabrication and investigation on the PANI/ MWCNT/thermally annealed graphene aerogel/epoxy electromagnetic interference shielding nanocomposites," *Compos. Part A*, vol. 121, pp. 265-272, 2019.
- [27] V. V. Bolotin, "Mechanics of delaminations in laminate composite structures," *Mech. Comp. Mat.*, vol. 37, pp. 367-380, 2001.
- [28] B. N. Cox, M. S. Dadkhah, W. L. Morris, and J. G. Flinto, "Failure Mechanisms of 3D woven composites in tension, compression and bending," *Acta Metall. Mater.*, vol. 42, pp. 3967-3984, 1994.
- [29] A. C. Long, "Design and manufacturing of textile composites," Woodhead Publishing Limited. Cambridge, England, 2005.
- [30] A. E. Bogdanovich, "Three-dimensional variational theory of laminated composite plates and its implementation with Bernstein basis functions", *Comp. Meth. App. Mech. Eng.*, vol. 185, pp. 279-304, 2000.
- [31] A. E. Bogdanovich, "Multi-Scale modeling, stress and failure analyses of 3-D woven composites." *J. Mater. Sci.*, vol. 41, pp. 6547-6590, 2006.
- [32] M. Pankow, A. Salvi, A. M. Waas, C. F. Yen, and S. Ghiorse, "Resistance to delamination of 3D woven textile composites evaluated using End Notch Flexure (ENF) tests: Experimental results," *Compos. Part A.*, vol. 42, pp. 1463-1476, 2011.
- [33] A. P. Mouritz, K. H. Leong and I. Herszberg, "A review of the effect of stitching on the in-plane mechanical properties of fibre-reinforced polymer composites," *Compos. Part A.*, vol. 28, pp. 979-991, 1997.
- [34] K. Maloney and N. Fleck, "Damage tolerance of an architected adhesive joint," *Int. J. Solids Struct.*, vol. 132, pp. 9-19, 2018.
- [35] X. K. Zhu, "Advances in fracture toughness test methods for ductile materials in low constraint conditions," *Proc. Eng.*, vol. 130, pp. 784-802, 2015.
- [36] C. Rubio, J. Wang and J. Martinez, "Dynamic fracture toughness of composite materials. In: Tamin M (ed.) *Damage and fracture of composite materials and structures. Advanced structured materials*, vol 17. Berlin, Heidelberg, Germany: Springer, 2012, pp. 143-156.
- [37] J. Zhang, S. Deng and L. Ye, "Composites with matrices modified by nano-silica and CTBN rubber. In: 13th international conference on fracture, Beijing, China, 16-21 June 2013, pp. 1-7. USA: Curran Associates, Inc.
- [38] G. Catalanotti, P. P. Camanho, J. Xavier, C. G. Davila and A. T. Marchques, "Measurement of resistance curves in the longitudinal failure of composites using digital image correlation," *Compos. Sci. Tech.*, vol. 70, pp. 1986-1993, 2010.
- [39] A. Ortega, P. Maimy, E. V. Gonzalez and L. Ripoll, "Compact tension specimen for orthotropic materials," *Compos. Part A: App. Sci. Manuf.*, vol. 63, pp. 85-93, 2014.

- [40] W. Tan, B. G. Falzon, M. Price and H. Liu, "The role of material characterization in the crush modelling of thermoplastic composite structures," *Compos. Struct.*, vol. 153, pp. 914-927, 2016.
- [41] M. V. Donadon, B. G. Falzon, L. Iannucci and J. M. Hodgkinson, "Intralaminar toughness characterization of unbalanced hybrid plain weave laminates," *Compos. Part A: App. Sci. Manuf.*, vol. 38, pp. 1597-1611, 2007.
- [42] F. Carrillo-Sanchez, G. Canche-Escamilla and P. J. Herrera-Franco, "A study of the fracture toughness of acrylic composites using the essential work of fracture method," *Polymer Testing*, vol. 29, pp. 565-571, 2010.
- [43] M. Marchetti, A. La Barbera and F. Morganti, "Fracture analysis of complex shaped structures by numerical and experimental methods," *Aeronautical J*, vol. 93, pp. 141-150, 1989.
- [44] N. Blanco, D. Trias, S. T. Pinho and P. Robinson, "Intralaminar fracture toughness characterization of woven composite laminates. Part I: Design and analysis of a compact tension (CT) specimen," *Eng. Fract. Mech.*, vol. 131, pp. 349-360, 2014.
- [45] P. Compston and P. Y. B. Jar, "Comparison of interlaminar fracture toughness in unidirectional and woven roving marine composites," *Appl. Compos. Mater.*, vol. 5, pp. 189-206, 1998.
- [46] A. F. Gill, P. Robinson and S. Pinho, "Effect of variation in fibre volume fraction on modes I and II delamination behavior of 5HS woven composites manufactured by RTM," *Compos. Sci. Tech.*, vol. 69, pp. 2368-2375, 2009.
- [47] T. K. O'Brien and R. H. Martin, "Results of ASTM round robin testing for mode I interlaminar fracture toughness of composite materials," *J. Compos. Tech. Res.*, vol. 15, 13 also in NASA TM 104222, 1992.
- [48] N. K. Naik, K. S. Reddy, S. Meduri, N. B. Raju, P. D. Prasad and S. N. M. Azad, "Interlaminar fracture characterization for plain weave fabric composites," *J. Mater. Sci.*, vol. 37, pp. 2983-2987, 2002.
- [49] A. Alif, L. A. Carlsson and L. Boogh, "The effect of weave pattern and crack propagation direction on mode I delamination resistance of woven glass and carbon composites," *Compos. Part B*, vol. 29, pp. 603-611, 1998.
- [50] W. S. Johnson and P. D. Mangalgari, "Investigation of fiber bridging in double cantilever beam specimens," *J. Compos. Tech. Res.*, vol. 9, pp. 10-13, 1987.
- [51] P. Davies, "Fracture of marine composites," *Key Eng. Mat.*, vol. 120, pp. 583-595, 1996.
- [52] R. H. Martin, "Delamination characterization of woven glass/polyester composites," *J. Compos. Tech. Res.*, vol. 19, pp. 20-28, 1997.
- [53] B. W. Kim and A. H. Mayer, "Influence of fiber direction and mixed-mode ratio on delamination fracture toughness of carbon/epoxy laminates," *Compos. Sci. Tech.*, vol. 63, pp. 695-713, 2003.
- [54] M. A. Jimenez and A. Miravete, "Application of the finite-element method to predict the onset of delamination growth," *J. Compos. Mat.*, vol. 38, pp. 1309-1335, 2004.
- [55] P. S. Valvo, "A revised virtual crack closure technique for physically consistent fracture mode partitioning," *Inter. J. Fract.*, vol. 173, pp. 1-20, 2012.
- [56] Y. Zhang and M. Chryssanthopoulos, "Modelling of mode I fracture behaviour of adhesively-bonded GFRP joints using virtual crack closure technique and cohesive zone method," 6th International Conference On Frp Composites In Civil Engineering, Rome, 2012.
- [57] J. Bonhomme, A. Argüelles, J. Vina and I. Vina, (2009). Numerical and experimental validation of computational models for mode I composite fracture failure," *Comp. Mater. Sci.*, vol. 45, pp. 993-998, 2009.
- [58] G. Barenblatt, "The mathematical theory of equilibrium cracks in brittle fracture. *Adv. App. Mech.*, vol. 7, pp. 55-129, 1962. DOI: 10.1016/j.ech.2007.03.012.
- [59] D. Dugdale, "Yielding of steel sheets containing slits," *J. Mech. Phys. Solids*, vol. 8, pp. 100-104, 1960. DOI:10.1016/0022-5096(60)90013-2.
- [60] G. Alfano and M. A. Crisfield, "Finite element interface models for the delamination analysis of laminated composites: mechanical and computational issues," *Int. J. Numer. Meth. Eng.*, vol. 50, pp. 1701-1736, 2001.
- [61] K. Park and G. H. Paulino, "Cohesive zone models: a critical review of traction-separation relationships across fracture surfaces," *Appl Mech Rev*, 64:060802-1-060802-20, 2011.
- [62] L. Škec, G. Jelenic and N. Lustig, "Mixed-mode delamination in 2D layered beam finite elements," *Int. J. Numer. Meth. Eng.*, vol. 104, pp. 767-788, 2015.
- [63] L. Škec, G. Jelenic, "Geometrically non-linear multi-layer beam with interconnection allowing for mixed-mode delamination," *Eng. Fract. Mech.*, vol. 169, pp. 1-17, 2017.
- [64] S. H. Song and G. H. Paulino and W. G. Buttlar, "Simulation of crack propagation in asphalt concrete using an intrinsic cohesive zone model," *J. Eng. Mech.*, vol. 132, pp. 1215-1223, 2006, DOI:10.1061/(ASCE)0733-9399(2006)132:11(1215).
- [65] Z. J. Zhang and G. H. Paulino, "Cohesive zone modelling of dynamic failure in homogeneous and functionally graded materials," *Inter. J. Plast.*, vol. 21, pp. 1195-1254, 2005. DOI:10.1016/j.ijplas.2004.06.009.
- [66] M. R. Khoshrovan and M. Moslemi, "Investigation on mode III interlaminar fracture of glass/epoxy laminates using a modified split cantilever beam test," *Eng. Fract. Mech.*, vol. 127, pp. 267-279, 2014. DOI:10.1016/j.engfracmech.2014.06.013.
- [67] S. H. Song, G. H. Paulino and W. G. Buttlar, "A bilinear cohesive zone model tailored for fracture of asphalt concrete considering viscoelastic bulk material. *Eng. Fract. Mech.*, vol. 73, no. 18, p. 2829-2848, 2006. DOI:10.1016/j.engfracmech.2006.04.030.
- [68] A. Turon, C. G. Davila, P. P. Camanho and J. Costa, "An engineering solution for mesh size effects in the simulation of delamination using cohesive zone models," *Eng. Fract. Mech.*, vol. 74, no. 10, p. 1665-1682, 2007. DOI:10.1016/j.engfracmech.2006.08.025.
- [69] H. Yuan and X. Li, "Effects of the cohesive law on ductile crack propagation simulation by using cohesive zone models. *Eng. Fract. Mech.*, vol. 126, pp. 1-11, 2014. DOI:10.1016/j.engfracmech.2014.04.019.
- [70] P. P. Camanho and S. R. Hallett, "Numerical modeling of failure in advanced composite materials; Woodhead Publishing: Cambridge, UK, 2015.

- [71] E.J. Barbero, “Finite Element Analysis of Composite Materials Using ANSYS, 2nd ed.; CRC Press Taylor & Francis Group: Boca Raton, FL, USA, 2014.
- [72] W. E. R. Krieger, Cohesive Zone Modeling For Predicting Interfacial Delamination in Microelectronic Packaging, Thesis MS.Eng, Georgia Institute of Technology, Atlanta, USA, 2014.
- [73] P.P. Camanho, C.G. Davila, and M. F. De Moura, “Numerical simulation of mixed-mode progressive delamination in composite materials,” *J. Compos.Mater.*, vol. 37, pp. 1415-1438, 2003.
- [74] M. L. Benzeggagh and M. Kenane, “Measurement of mixed-mode delamination fracture toughness of unidirectional glass/epoxy composites with mixed-mode bending apparatus,” *Compos.Sci.Tech.*, vol. 56, pp.439-449, 1996.
- [75] D. F. Devitt, R. A. Schapery and W. L. Bradley, “A method for determining the mode I delamination fracture toughness of elastic and viscoelastic composite materials,” *J. Compos. Mater.*, vol. 14, pp. 270–285, 1980. <http://dx.doi.org/10.1177/002199838001400401>.
- [76] J. G. Williams, Large displacement and end block effects in the ‘DCB’ interlaminar test in modes I and II,” *J. Compos. Mater.*, vol. 21, pp. 330–47, 1987. <http://dx.doi.org/10.1177/002199838702100403>.
- [77] J. Czabaj and G. Ratclie, “Comparison of intralaminar and interlaminar Mode I fracture toughnesses of a unidirectional IM7/8552 carbon/epoxy composite,” *Compos. Sci. Tech.* vol.89, pp. 15–23, 2013.

# Tilapia Powered Aquaponics to Optimize Land and Water Use for Safe Food Production from the Rooftop

M. A. Salam<sup>1</sup>, Tania Islam<sup>2</sup>, Zubyda Mushtari Nadia<sup>3</sup>

<sup>1</sup>Department of Aquaculture, Faculty of Fisheries, Bangladesh Agricultural University, Mymensingh-2202, Bangladesh

<sup>2</sup>Department of Fisheries and Marine Biosciences, Bangabandhu Sheikh Mujibur Rahman Science and Technology University, Gopalganj, Bangladesh

<sup>3</sup>Department of Aquatic Animal Health Management, Sher-e-Bangla Agricultural University, Dhaka- 1207, Bangladesh

**Abstract**—Tilapia powered vertical aquaponics system (TPVAS) is an effective way to increase crop production in a food desert city per unit rooftop area by extending crop cultivation into the vertical dimension to feed the ever-increasing population of the world and keep the city-pollution free and cooler. Experiments conducted over the years to assess the viability of tilapia powered lettuce, strawberry, water spinach and mint production in the media-based vertical aquaponics system at the rooftop and lab of Bangladesh Agricultural University, Mymensingh, Bangladesh. The wastewater of the tilapia tank irrigated to the 4 feet height and 3-4-inch diameter vertical plastic pipes holding 15 to 18 saplings in each pipe which passing through the coco dust, coco coir, water hyacinth root, and brick chips media then return into the fish tank again. Fish growth performances, nutrients availability, and their use assessed. The mean length and weight gain of tilapia were 2.95 ( $\pm 0.83$ ) to 11.77 ( $\pm 2.49$ ) cm and 32.71 ( $\pm 9.43$ ) to 170.38 ( $\pm 78.7$ ) g. The feed conversion ratio (FCR) were 2.5, 2.35, 2.33 and 1.5 and survival rates were 96, 78, 85 and 98.33% for lettuce, strawberry, water spinach and mint based tilapia aquaponics systems. The fish and vegetable production was 30.64 to 135.20 and 12.47 to 123.25 MT/ha/90 to 120 days respectively. Among the four media, coco coir produced the highest crop than the others. Therefore, it is concluded that the TPVAS is suitable and capable of producing fish and vegetables at the rooftop keeping the rooftop cooler and greener than nearby traditional roof gardening buildings.

**Keywords**—Fish well-being, Rooftop, Safe food, Tilapia, Vertical aquaponics.

## I. INTRODUCTION

The world population will reach 9.6 billion by 2050, 34 percent higher than the present population. Most of the population increase will occur in developing countries like Bangladesh (Kodmany, 2018) where agricultural land is shifting to other uses day by day. Global food production will face great challenges in the future as the rice-growing field has decreased by 18% from 1971 to 2015 (BBS, 2016; Christine and Gruda, 2015). Moreover, the natural calamities like cyclones, tornadoes, droughts, floods and river erosion destroys a significant amount of crops each year that threatened food security in the country. In addition, huge demand for seeds and fertilizers, higher transport costs, burning fossil fuel, and climate change impact are responsible for price hick of agricultural commodities in the country (Hugh, 2016) The scientists emphasized to grow food in the cities at the vicinity of the consumers to cut the transport costs and address climate change impact (Paxton, 1994; Wakeland, 2012).

Bangladesh is one of the world's leading fish producing countries with a total production of 4.134 million tons, where inland fisheries contributed 82.26% comprising 29.34% from capture fisheries and 52.92% from aquaculture (DoF, 2018). The fisheries sector plays an important role in lessening malnutrition, earning foreign exchange and improving the socioeconomic status of the rural small farmers of Bangladesh (Uddin and Farjana, 2012). Fish supply 60% animal protein to the countrymen and support the livelihoods of 11-12% fishermen (FAO, 2012). The country ranked 3rd place among the inland water fish producing countries and 5th in aquaculture (FAO, 2018). The farmers expanding aquaculture activities horizontally not addressing the environmental pollution and shortage of land (Marco and Kuenzer, 2016). In such a situation, environmental engineering and eco-friendly farming the "Tilapia Powered Vertical Aquaponics System" (TPVAS) can a substitute to resolve the problems (Katy, 2019). The TPVAS has been increasing popularity as a way to reduce the need for arable land and grow crops where they are to be consumed. When farming indoors, on rooftops and balcony in a closed or semi-closed environment, the plants are protected from the bad weather, insects, and pests (Liu *et al.*, 2016). There are no losses of nutrients in closed systems and water use is less in comparison to traditional farming. However, artificial lighting is

necessary while crops grow indoor. Additionally, TPVAS is capital intensive and requires knowing how to handle the new techniques and maintenance. The system combines ecology and environmental engineering to solve existing problems as well as address land crisis through utilizing unused space, beautifying the backyard and rooftop in a cost-effective and ecosystem approach (Kangas, 2004; Kheir, 2018).

Mint (*Mentha arvensis*) is a native aromatic herb which used to enhance the flavor of food in time immemorial as a component of the traditional drug for therapeutic purposes (Normala *et al.*, 2010). From ancient time, the mint has played an important role in trade due to its diverse elements and applications (Sahil *et al.*, 2011). It is famous as an indigenous herb in the Indo-Pak subcontinent for its well-being, taste, essential oil and defensive potential (Baliga and Rao, 2010). The mint contains moisture, protein, fat, minerals and vitamins, fibers and carbohydrate of 78.65, 3.75, 0.94, 0.9, 8.0, and 14.89% respectively. It also contents 70 Kcal of energy (The USDA National Nutrient Database, 2011). Moreover, the mint has been widely used as a traditional medicine for the treatment of anorexia, nausea, flatulence, bronchitis, colitis ulcer and liver anomalies due to its various health promoter activities (Hadjlaoui *et al.*, 2009). The leaves and essential oil are the dominant use of mint (Beemnet *et al.*, 2010; Verma *et al.*, 2010; Gul, 1994). By contrasts, strawberry (*Fragaria ananassa*) is bright red, juicy, sour and sweet in taste and rich in antioxidants and full of plant compounds that help to control heart health and blood sugar level. It is also an excellent source of vitamin C and manganese and has a small amount of folate (vitamin B9) and potassium. It is usually consumed raw and fresh, the berry can also be used in a variety of value-added products like jam, jelly, and dessert (Halvorsen *et al.*, 2006; Giampieri *et al.*, 2012). The lettuce (*Lactuca sativa*) is another favorite green leafy vegetable that is popular worldwide and consumed raw in salad and burger. It is crunchy and green which has many essential nutrients for health benefit (Liu, 2003; Pandey and Rizvi, 2009). In Addition, the leafy vegetable water spinach (*Ipomoea aquatica*) is also popular green vegetable which is rich sources of fiber, vitamins, and minerals (Anderson *et al.*, 1994). Water spinach is a vegetable plant which has decent nutraceutical uses and is commonly eaten as a vegetable and mostly found in tropical and sub-tropical Asia, Indian sub-continent, Africa and Australia (Chitrajit and Pinak, 2015). Therefore, lettuce, strawberry, water spinach, and mint production experiments carried out in media-based TPVAS for integrated nutrient management, ease pressure on land resources and produce organic fruits and vegetables which have improved the physical, chemical and biological properties of soil less crop production as well as increased production from an unproductive unit of the rooftop area.

## II. MATERIALS AND METHODS

### 2.1 Experimental site and set up

The experiments were carried out during a period of 90 to 125 days from 2014 to 2017 at the backyard “Aquaponics Oasis” laboratory and rooftop, Department of Aquaculture, Bangladesh Agricultural University (BAU), Mymensingh. Among different types of aquaponics systems, the media-based vertical aquaponics system selected to carry out the researches. The experimental design composed of twelve fish holding tanks, a 4-inch diameter 3 ft. long 48 PVC pipes, coconut coir, coco fiber, water hyacinth roots and brick chips as the growing media (Fig. 1). Four different types of media, coco dust and coco coir (T1 and T2), water hyacinth root (T3) and brick chips (T4) each having three replication used in those experiments to grow lettuce, strawberry, water spinach, and mint. Fifteen to eighteen holes at an equal distance created with the hole saw drill machine in each pipe. The pipes containing various media were hung from the above with a parallel bamboo pole in rows following completely randomized block design (CRBD), indicated as T<sub>1</sub>R<sub>1</sub>, T<sub>1</sub>R<sub>2</sub>, T<sub>1</sub>R<sub>3</sub>, T<sub>2</sub>R<sub>1</sub>, T<sub>2</sub>R<sub>2</sub>, T<sub>2</sub>R<sub>3</sub>, T<sub>3</sub>R<sub>1</sub>, T<sub>3</sub>R<sub>2</sub>, T<sub>3</sub>R<sub>3</sub>, T<sub>4</sub>R<sub>1</sub>, T<sub>4</sub>R<sub>2</sub>, and T<sub>4</sub>R<sub>3</sub>. Twelve 750 L capacity plastic water tanks used as the fish holding tanks in all the four treatments. An inlet and outlet pipes set and connected with the PVC pipes in all the treatments. Twelve 25-watt submersible pumps used to pump the fish tank water to the vertically set pipes having the growing media in each treatment. An air pump with air stones provided oxygen to the fish tanks for fish well-being.

The plastic water tank in each treatment cut off the upper part and washed properly for keeping the fish in. After setting the tank, a layer of 3-4-inch brick let's put at the bottom of the tank. The inlet and outlet pipes (Fig. 1) were plumber to pump the fish tank water to the vertical pipes. The hanging pipes in all the treatments filled with locally procured coconut coir, coco fiber, water hyacinth roots, and brick chips. Then all the (48) pipes hung from a horizontal bamboo pole at a sun-exposure spot at the rooftop of a building at BAU and “BAU Aquaponics Oasis” laboratory.

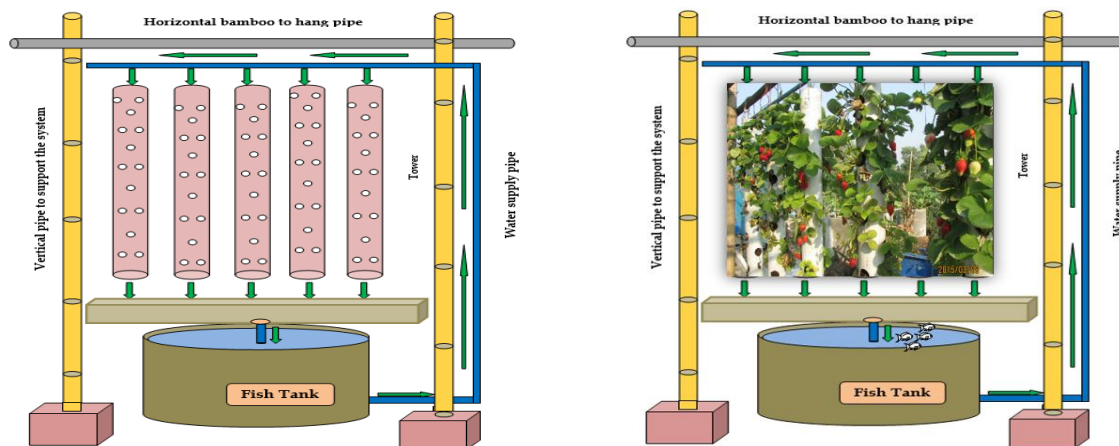


**FIGURE 1: Experimental design with vertical pipe having 15 to 18 holes each in a 3 feet long pipe, water inlet and out let system in left and fruiting strawberry and fish in tank at right.**

The healthy saplings of lettuce, strawberry, water spinach and mint of 6.5-10 cm size each planted in each hole in the pipes. In all the four treatments, the saplings uprooted from the soil or germinating pot and washed well with clean water before being transplanted into the pipes. Followed by planting the saplings, mono sex tilapia (181 fish/m<sup>3</sup> water) juveniles (*Oreochromis niloticus*) of 7.76 ( $\pm$  2.14) to 15.26( $\pm$ 1.41) cm and 3.83( $\pm$  1.10) to 60.06( $\pm$ 17.69) g initial length and weight collected locally and released in each fish tank. Thirty percent protein-containing commercial floating pellet feed fed twice daily, at 9:00 AM and at 5:00 PM at the rate of 5% of fish body weight in 1st month, then the feeding rate was re-adjusted to 3 and 2% in 2nd and 3rd month. Fish tank water was irrigated with a submersible pump from the fish tank to the vertical pipes from the upper side which then passes through the pipes and finally falls in the fish tank again. The water pumps operated in the daytime only. The irrigation pipes, water pumps, air tubes, and air stones cleaned regularly to avoid clogging with algae and fish poo. No weeding was essential in the system; however, if there were any weed seen, they removed instantly.

## 2.2 Sampling the fish and vegetable and harvesting

The lettuce, strawberry, water spinach, and mint sampling carried out fortnightly but 1st harvest of lettuce, water spinach, and mint carried out after one month and strawberry harvested when ripe fruits were available. Following the harvest, their length, number of branches, leaf number and weight measured and recorded. Ten fishes sampled randomly caught from each replication of each treatment using a handheld scoop net. Length and weight of the fish measured with care and data recorded in the notebook and transferred into the computer later. The fish and all the vegetables were finally harvested after 90-125 days of the experiment. The length and weight gain calculated after harvest and % length gain and % weight gain, specific growth rate (SGR), feed conversion ratio (FCR), survival and fish production were also calculated.

## 2.3 Sampling water parameters

Physio-chemical parameters of fish tank water such as dissolved oxygen (DO), temperature and pH measured bi-weekly. The Sera water testing kits and Hanna® pH/Ec/TDS/DO meters used to sample the physio-chemical parameters of water. In addition, total nitrogen (Total-N), electric conductivity (EC), carbonate (CO<sub>3</sub><sup>2-</sup>), hydrogen carbonate (HCO<sub>3</sub><sup>-</sup>), potassium (K), sulfur (S), sodium (Na) and phosphorus (P) also measured twice during the experiment in all the treatments, 1st at the beginning and last at the end of the experiment at the Humboldt Soil Testing Laboratory, Soil Science Department, BAU.

## 2.4 Data processing and analysis

All the collected data were recorded and transferred into the computer and cross-checked for any mistake. The data were converted into a Microsoft Excel master sheet and prepared the tables and graphs. One-way ANOVA performed on the collected data using XI-stat at a 95% significance level. Tukey's HSD (Honestly Significant Difference), Duncan's multiple range test and Fisher's LSD (Least Significant Difference) tests performed to test significant differences in triplicate and across the treatments means.

### III. RESULTS AND DISCUSSION

#### 3.1 Water quality parameters

Mint and water spinach experiments conducted in the summer when the environmental temperature was higher. On the other hand, lettuce and strawberry experiments conducted in winter from November to March from 2014 to 2017 when the temperature was lower than the rest of the year. The range of pH, temperature and dissolved oxygen of the water in the fish tank recorded throughout the culture period of 7.56(±0.19) to 7.83(±0.14), 21.56(±3.26) to 29.70 (±1.21)°C and 3.86(±0.04) to 4.80 (±0.02) ppm. The minimum pH value was 7.30 on 25th January, 22nd February and 29th March, 2015. By contrast, the minimum and maximum water temperature were 14°C on 28th January 2015 in lettuce based tilapia production system and 29.70 (±1.21) °C on 4 September 2014 (Table 1). The present results suggested that a favorable range of pH for both fish and nitrifying bacteria in a vertical aquaponics system existed. The literature revealed that the pH range of 6.5 – 8.5 is appropriate for tilapia culture (Swingle, 1968; Huet, 1972; Makori *et al.*, 2017), while, the nitrifying bacterial growth is withdrawn below the pH of 6.5 with an optimum pH of 7.8 favorable on species and temperature (Tyson *et al.*, 2007; Alenka *et al.*, 1998). The range of water temperature found in present experiments imitates the suitable range for tilapia culture and nitrifying bacteria in the aquaponics system (Wortman and Wheaton, 1991; Rahmatullah *et al.*, 2010).

TABLE 1

Nutrient profile of influent and effluent water in water spinach tilapia based vertical aquaponics system

Parameters	July-2014		August-2014	
	Influent	Effluent	Influent	Effluent
<b>P (ppm)</b>	0.832 (±0.11) <sup>c</sup>	0.398 (±0.03) <sup>d</sup>	1.686 (±0.11) <sup>a</sup>	1.191 (±0.11) <sup>b</sup>
<b>K (ppm)</b>	15.13 (±1.14) <sup>a</sup>	15.53 (±1.18) <sup>a</sup>	14.5 (±2.14) <sup>a</sup>	4.632 (±0.74) <sup>b</sup>
<b>S (ppm)</b>	3.509 (±0.16) <sup>b</sup>	3.709 (±1.19) <sup>b</sup>	8.96 (±1.16) <sup>a</sup>	1.67 (±0.19) <sup>c</sup>
<b>Na (ppm)</b>	43.99 (±7.17) <sup>a</sup>	43.99 (±1.21) <sup>a</sup>	39.531 (±2.11) <sup>b</sup>	37.95 (±1.17) <sup>b</sup>
<b>HCO<sub>3</sub><sup>-</sup></b>	189.1 (±17.13) <sup>b</sup>	195.2 (±1.2) <sup>b</sup>	219.6 (±28.13) <sup>ab</sup>	256.2 (±51.13) <sup>a</sup>
<b>CO<sub>3</sub><sup>2-</sup> (ppm)</b>	72 (±6.12) <sup>a</sup>	36 (±1.12) <sup>b</sup>	12 (±2.12) <sup>c</sup>	42 (±9.12) <sup>b</sup>
<b>Total N (ppm)</b>	4.2 (±1.15) <sup>b</sup>	3.2 (±0.15) <sup>b</sup>	11.2 (±1.15) <sup>a</sup>	5.6 (±1.15) <sup>b</sup>
<b>EC (µc/cm)</b>	394 (±47.17) <sup>b</sup>	338 (±31.21) <sup>b</sup>	598 (±37.17) <sup>a</sup>	391 (±58.17) <sup>b</sup>

*The values in the same column having similar letter (s) do not differ significantly, whereas, values bearing the dissimilar letter (s) differ significantly as per Duncan's multiple range tests. Values in the parenthesis indicate the standard error.*

The nutrient values in the effluent water were lower than in the influent water in all the four vertical aquaponics system. However, the difference was sometimes significant and sometimes not in Fisher's LSD test (Table 1 and 2). The highest EC recorded in influent water in August 2014 (598 ±37.17) and May-2016 (662±2.83) in spinach-tilapia and mint-tilapia based vertical aquaponics system. Moreover, the nutrients had significantly or not significantly reduced in the effluent water at the end of the experiments because the plants extracted enough nutrients for their growth from the water at their growth stage. Werner *et al.* (2015) reported EC of 526.73 -753.53 (± 125.30) µc/cm in an aquaponics experiment in a greenhouse environment which is more or less similar to the present study.

The amount of carbonate and total-N were higher at the beginning but reduced significantly at the end of the experiment. However, carbonate had increased again in the effluent water at the end of the experiment, possibly the extraction reduced by mint and water spinach from the water. The total-N, potassium, sulfur and sodium concentrations were gradually increased with the time passes but reduced again in the effluent water towards the end of the study, suggesting that these nutrients extracted by the plants at a higher rate for their growth. However, the phosphorus extraction in later stages was less in comparison to production in the last sampling in August 2014 in the mint tilapia co-production system. But in the strawberry tilapia co-production system, initially, phosphorus concentration was low and with the time passed it was in a peak and later plants consumed and concentration reduced again (Fig. 2). The concentration of hydrogen carbonate, however, increased throughout the experimental period and a significantly higher amount recorded at the end of the study. It was not clear whether plants had used hydrogen carbonate or not (Table 1).

**TABLE 2**  
**AVAILABLE NUTRIENTS IN INFLUENT AND EFFLUENT WATER IN MINT BASED TILAPIA VERTICAL AQUAPONICS SYSTEM**

Parameters	Influent			Effluent		
	May-2016	June-2016	July-2016	May-2016	June-2016	July-2016
<b>P(ppm)</b>	0.16±0.01	0.93±0.01	1.73±0.03	0.06 ±0.001	0.53±0.002	1.61±0.04
<b>K (ppm)</b>	6.12±0.28	5.27±0.01	5.75±0.14	6.02±0.42	0.84±0.04	4.64±0
<b>S (ppm)</b>	0.49±0.01	4.52±0.30	4.03±0.04	0.27±0.01	3.33±0.25	3.71±0.33
<b>Na (ppm)</b>	64.15±1.4	23.71±0.01	29.4±0	60.0±1.12	23.64±0.06	29.2±0.28
<b>HCO<sub>3</sub><sup>-</sup></b>	219.6±8.63	140.3±34.51	216.55±4.31	253.15±12.94	140.3±8.63	192.15±4.31
<b>CO<sub>3</sub><sup>2-</sup> (ppm)</b>	0.0	34.5±2.12	0.0	0.0	22.5±2.12	0.0
<b>Total-N (ppm)</b>	4.9±0.99	22.15±0.35	29.4±1.98	2.8±0	17.05±0.35	25.2±0
<b>EC (µs/cm)</b>	662.0±2.83	567.0±1.41	574.5±3.54	666.0±5.66	489.0±1.41	549.5±0.71

*Note: Values are given with ± standard deviation*

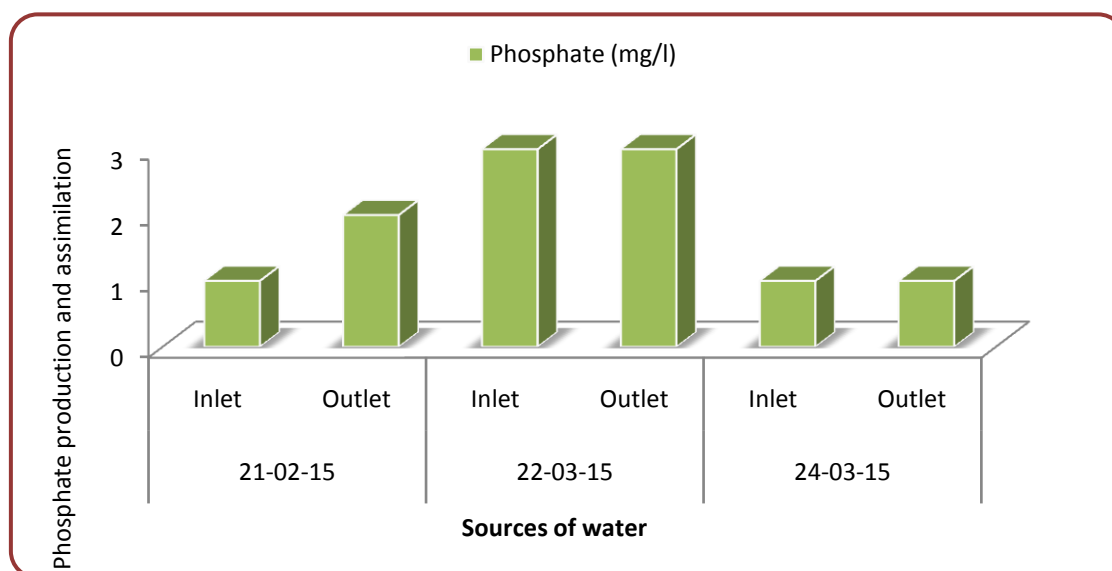


**FIGURE 2: Phosphorus production and assimilation in strawberry tilapia based vertical aquaponics system.**

In tilapia –mint-based vertical aquaponics system, the fish produced wastes that help as manure for plants' growth and clean water revenues to the fish tank again. The highest value of phosphorus (P) was 1.69(±0.11) ppm in influent, that reduced to 1.19(±0.11) ppm in the effluent water. In the system, 52% P removal was found in the earlier stage of the experiment that was 29.5% at the end. It is distinguished that primarily the P absorption in the influent water was slower in earlier than in later stage and removal was higher. However, in the later stage the P concentration increased and plants absorbed it according to their need that speed up the extraction level higher. Ghaly *et al.* (2005) reported 91.8 to 93.6% P reduction in aquaponics system where they grow barley as a vegetable. Boyd (1998) reported the acceptable P level in aquaponics systems was 0.20-1.15 ppm. Hence, the phosphorous level in the tilapia–mint-based vertical aquaponics system was within the range of the above findings. In addition, the potassium and sulfur concentrations in effluent were higher than in the influent at the beginning of the study. However, at the end of the experiment, when the plants reached maturity, the concentrations of the effluent reduced significantly than the influent concentrations in the system. On the contrary, sodium content was remained static in influent and effluent water at the start of the experiment, nonetheless gradually which decreased with the progress of the study, suggesting that the plants might need a bit of sodium for their growth. The nutrient concentrations in the system were lower than the soil which are generally acceptable for aquaponics as nutrients derived from an excess feed provided to the fish in the tank, and small amounts of nutrients added from the fish feces and mineralization of organic matter (Bittsánszky *et al.*, 2016; Rakocy *et al.*, 2004).

### 3.2 Fish growth and production

In tilapia based vertical aquaponics system, initial mean length and weight of tilapia were 13.74( $\pm$ 1.77), 22.21( $\pm$ 5.72), 9.06 ( $\pm$ 1.22) and 15.26 ( $\pm$ 1.41) cm and 51.13 ( $\pm$ 22.27), 244.83 ( $\pm$ 167.01), 17.27 $\pm$ 6.50 and 60.06 ( $\pm$ 17.69) g in tilapia based lettuce, strawberry, water spinach and mint vertical aquaponics system individually. During harvest, the highest mean length gained 11.77 ( $\pm$ 2.49) with tilapia-water spinach system followed by 5.51 ( $\pm$ 0.14), 2.98( $\pm$ 1.05) and 2.95( $\pm$ .83) g with mint, strawberry, and lettuce VAS respectively (Figs. 3 & 4). By contrast, the highest mean weight gained was 170.38( $\pm$ 78.7) g followed by 114.54 ( $\pm$ 28.18), 73.91( $\pm$ 15.95), and 58.92( $\pm$ 52.80) g in tilapia based lettuce, strawberry, water spinach, and mint vertical aquaponics systems.

The highest FCR (2.54) was found with tilapia-lettuce followed by tilapia-strawberry (2.35) system. However, the least FCR found with a tilapia-mint vertical aquaponics system. Ashraf *et al.* (2015) reported FCR of 1.69 and 1.80 for Nile tilapia production in the aquaponics system. Moreover, Azimuddin *et al.* (1998) reported FCR of 1.73 to 2.04 for tilapia fed formulated feed. The above findings are more or less match with the present study. Besides, the highest fish survival was 98.33% found in mint-based vertical aquaponics system followed by 96% with the tilapia-lettuce system and the lowest survival was found with Tilapia Strawberry vertical aquaponics system. The highest fish production (135.2 MT/ha/90 days) was with mint based vertical aquaponics system trailed by tilapia based water spinach vertical system where production was 134.3MT/ha/116 days but if we consider the duration of production then we can see tilapia-mint based vertical system produced 135.2MT/ha in only 90 days.



**FIGURE 3: Tilapia based lettuce in VAS**



**FIGURE 4: Tilapia based Mint in VAS**

The lettuce production was the highest (107.89 MT/ ha/116 days) in tilapia lettuce based vertical aquaponics system, followed by 46.08 MT /120 days and 83.91 MT / 116 days' strawberry and water spinach. Moreover, the lowest vegetable production was 12.47 MT mint/ha/120 days (Table 3). The vertical farming systems (VFS) increase crop production into vertical dimension and not horizontal to achieve a higher revenue using less area (Hochmuth and Hochmuth, 2001; Resh, 2012). Moreover, yield increases about 129–200% in VFS and a profit increase of 3.6–5.5 US dollar/m<sup>2</sup> area compared to traditional soil cultivation (Liu *et al.*, 2004). Therefore, we can see the vertical farm offers more opportunities considering the three pillars of sustainability- environment, society, and economy (Kheir, 2018).

In the tilapia-mint based vertical aquaponics system, for a one cm length increase of fish, the weight increased on an average 19.91 g. Tukey's (HSD) test showed significant differences in mean length and weight of fish between few sampling dates but not all the dates. The Coefficient of determination, ( $R^2$  value) was 0.982, signifying that 98% of the variation of the dependent variable (weight) explained by the independent variable (length). The positive correlation ( $r=0.99$ ) between the length and the weight of tilapia was very high. The mean food conversion ratio in the experiment was 1.50, survival was 98.33%, % length gain 36.11( $\pm$ 9.93), % weight gain 190.71 ( $\pm$ 159.29) and total production of tilapia were 135.20 MT/ha/90 days (Table 3). Higher rates of  $\text{CO}_3^{2-}$  reduction (72.00 $\pm$ 6.12 to 36.00 $\pm$ 1.12 ppm) noticed in the system in July 2016, while the value increased significantly in the effluent in August 2016. On the other hand, the  $\text{HCO}_3^-$  level gradually increased over the

culture period as plants didn't take up the carbonate at a significant level. A similar result obtained by Salam *et al.* (2014). Rahmatullah *et al.* (2010) and Quagraine *et al.* (2011) reported FCR of 2.69 and 3.10 in tilapia rearing in aquaponics system and pond condition.

The lowest total-N removal from the influent was 23% in the present study ( $4.20 \pm 1.15$  to  $3.20 \pm 0.15$  ppm) observed in July, because the highest removal from the system was 50% in August. Ghaly and Snow (2008) reported 76% of total-N removal with Arctic charr (*Salvelinus alpinus*) based aquaponics system and Endut *et al.* (2011) stated  $\text{NO}_3\text{-N}$  removal of 79.17% and 87.10% after 4 and 12 week for the water spinach system, all the above findings were higher than the present findings.

The EC is the measurement of electric current moves through the water. The current can only move through water when there is some salt dissolved in water, but cannot move through pure water. A greater amount of salt dissolved in the water, higher EC and higher nutrient concentrations in water result in superior growth of plants (Pantanella, 2012). The EC value decreased in the effluent throughout the culture period. The highest EC value was  $598.00 (\pm 37.17)$   $\mu\text{c}/\text{cm}$  in inlet water, which reduced to  $338.00 (\pm 31.21)$   $\mu\text{c}/\text{cm}$  in the outlet that means removal was 56.52%. Kim (2018) mentioned that vegetable types control the water quality and he found  $523 \pm 18$ ,  $832 \pm 43$  and  $912 \pm 52$  EC in tomato, basil and lettuce based aquaponics system. The current results are evidence of nutrient removal from the fish tank water used by the mint for their growth.

In the tilapia-water spinach based vertical aquaponics system, tilapia reared for 116 days in a 750-liter plastic water tank where mean length gain was  $11.77 (\pm 2.49)$  cm and mean weight gain was  $170.38 (\pm 78.7)$  g at harvesting (Table 3). Midmore (2011) reported the mean weight gain of tilapia was  $85.39 \pm 12.04$  g after 180 days of raising which is much lower than the present findings due to the seasonal variation, rearing condition and better feed and feeding regime used in the present study.



**FIGURE 5: Tilapia based strawberry VAS**

The FCR values were 2.54, 2.35, 2.33 and 1.5 in tilapia-lettuce, Tilapia-Strawberry, tilapia-water spinach, and tilapia-mint based vertical aquaponics systems. Rahmatulla *et al.* (2010) reported FCR of 2.19 to 2.69 in the tilapia based aquaponics system and Watanabe *et al.* (2002) mentioned the anticipated FCR of 1.5-2.0 for table size tilapia production. The FCR of the present study more or less similar to the above mention results but some of the FCR higher might be due to unfavorable temperature, feed loss, and some experimental mistakes. Additionally, specific the growth rate achieved 0.98 g, survival rate 85% and total fish production 134.30 MT/ha/116 days which matched with the findings of Salam *et al.* (2014) where they reported tilapia production of 130 MT/ha/116 days in the vertical aquaponics system.

**TABLE 3**  
**GROWTH PERFORMANCES OF TILAPIA BASED LETTUCE, STRAWBERRY, WATER SPINACH, MINT CO-PRODUCTION SYSTEMS**

Growth Parameters of tilapia based systems	Lettuce	Strawberry	Water spinach	Mint
Mean Initial Length (cm)	13.74(±1.77)	22.21 (± 5.72)	9.06±1.22	15.26 (±1.41)
Mean Final Length (cm)	16.69 (±2.60)	25.19 (±4.98)	20.83 (±3.04)	20.77 (±1.55)
Mean Length Gain (cm)	2.95 (±.83)	2.98 (±1.05)	11.77(±2.49)	5.51 (±0.14)
Percent Length Gain (%)	21.47	13.43 (± 18.47)	231.29 (±28.10)	36.11 (±9.93)
Mean Initial Weight (g)	51.13 (±22.27)	244.83 (±167.0)	17.27 (±6.50)	60.06 (±17.69)
Mean Final Weight (g)	125.04(±38.22)	303.75(±180.6)	187.65(±81.93)	174.6 (±45.87)
Mean Weight Gain (g)	73.91(±15.95)	58.92 (±52.80)	170.38 (±78.7)	114.54 (±28.18)
Percent Weight Gain (%)	144.55(±50.60)	43.95(± 39.28)	1161(±526.8)	190.71(±159.3)
Specific growth rate (SGR)	96.0	0.27	0.98	0.83
Feed conversion ratio (FCR)	2.54	2.35	2.33	1.5
Survival rate (%)	96	78	85	98.33
Fish density /m3	67 (104)	100 (150)	107	80
Fish production (MT/ha)	47.33/105days	30.64/120 days	134.3/ 116 days	135.2/90 days
Vegetable production(MT/ha)	107.89/105days	46.08 /120 days	83.91/ 116 days	12.47 /90 days

**TABLE 4**  
**LENGTH (CM) AND WEIGHT (G) MEASUREMENT OF FISH IN TILAPIA-MINT BASED VERTICAL AQUAPONICS SYSTEM IN DIFFERENT SAMPLING DATES**

Dates	Length of Tilapia (cm)	Weight of Tilapia (g)
4 <sup>th</sup> June 2014	15.26 (±1.41) <sup>c</sup>	60.06 (±17.69) <sup>d</sup>
19 <sup>th</sup> June 2014	16.09 (±0.96) <sup>c</sup>	77.39 (±15.95) <sup>d</sup>
4 <sup>th</sup> July 2014	16.72 (±1.66) <sup>c</sup>	83.55 (±28.96) <sup>d</sup>
19 <sup>th</sup> July 2014	17.21 (±1.59) <sup>bc</sup>	90.71 (±24.77) <sup>cd</sup>
4 <sup>th</sup> August 2014	19.04 (±1.59) <sup>ab</sup>	129.90 (±34.21) <sup>bc</sup>
19 <sup>th</sup> August 2014	19.50 (±1.66) <sup>a</sup>	134.50 (±37.55) <sup>ab</sup>
4 <sup>th</sup> September 2014	20.77 (±1.55) <sup>a</sup>	174.60 ±45.87) <sup>a</sup>

#### IV. CONCLUSION

Vertical aquaponics system proved highly successful in producing vegetables in a small area even from the rooftop. With the shortage of suitable farming land in urban sprawl, rooftops are progressively being seen as a reasonable place for producing food and make the building a sustainable food production unit in the future for cities. Like most of the cities in our country an abundance of fallow rooftop places are prevails. The present experiment used four different types of vegetable tilapia in vertical aquaponics system which performed well; nevertheless, water hyacinth root performed better than the coconut coir, coco fiber and brick chips. The system efficiently recycles the fish tank wastewater and uptake nutrients to grow crops compared to the conventional system, therefore, the vertical aquaponics system could potentially help to enhance food and nutrient security and reduce pressure on land resources. In this amazing food growing technology, the fish acts as the powerhouse of vegetable production. Aquaponics already proved as a green, sustainable and eco-friendly food

growing technology, hence, vertical aquaponics will be able to feed the 21st century's 8.3 to 9.0 billion people and safeguard the environment for the future generation.

### ACKNOWLEDGEMENTS

The authors are thankful for the financial support by BAS-USDA PALS/2017/282 (Bangladesh Academy of Science- United States Department of Agriculture) Project. The authors also express their gratitude to the staff of "Fish Nutrition Laboratory", Department of Aquaculture, Bangladesh Agricultural University (BAU), Mymensingh and "Laboratory of Soil Science Division", Bangladesh Agricultural Research Institute (BARI), Joydebpur, Gazipur for their support to carry out proximate composition and other chemical analyses of the samples.

### REFERENCES

- [1] AlenkaPrinčič, Ivan Mahne, France Megušar, Eldor A. Paul, James M. Tiedje. 1998. Effects of pH and Oxygen and Ammonium Concentrations on the Community Structure of Nitrifying Bacteria from Wastewater. *Appl Environ Microbiol.* 64(10): 3584–3590.
- [2] Anderson J., Smith B. and Gustafson N. 1994. Health benefits and practical aspects of high-fiber diets. *Am. J. Clin. Nut.* 59(5):1242-1247.
- [3] Ashraf M. A-S Goda, Mohamed A. Essa, Mohamed S. Hassaan, ZakiSharawy.2015. Bio Economic Features for Aquaponics Systems in Egypt. *Turkish Journal of Fisheries and Aquatic Sciences* 15: 525-532.
- [4] Azimuddin K. M. 1998. Effect on stocking density on the growth of Thai pangus, *Pangasiussutchi* (Folwer) in net cage by using formulated diet, MS Thesis, Department of Aquaculture, Bangladesh Agricultural University, Mymensingh. pp.1-62.
- [5] Baliga M. S., and Rao S. 2010. Radio protective potential of mint: a brief review. *Journal of Cancer Research and Therapeutics*, 6, 255-262.
- [6] Bangladesh Bureau of Statistics (BBS). 2016. Statistical Yearbook of Bangladesh, Statistics and Informatics Division (SID) Ministry of Planning.
- [7] Beemnet O. M., Tsion T., and Solomon A. 2010. Production, processing and utilization of aromatic plant. *Ethiopian Institute of Agricultural Research Institute (EIAR), Addis Ababa, Ethiopia* (pp. 31).
- [8] BittsánszkyAndrás, NikolettUzinger, Gabor Gyulai, TamasKomives, Benz Kotzen, Morris Villarroel, RankaJunge and Alex Mathis. 2016. Nutrient supply of plants in aquaponics systems. *Ecocycles*, 2(2): 17-20.
- [9] Boyd, C.E. 1998. Water quality in ponds for aquaculture. *Research and Development Series. Number 43. International Centre for Aquaculture and Aquatic Environments, Alabama Agricultural Experimental Station, Auburn University, Alabama*, pp: 402.
- [10] ChitrajitMalakar and PinakPaniNath Choudhury. 2015. Pharmacological Potentiality and Medicinal Uses of *Ipomoea Aquatica*Forsk: A Review, *Asian J. Pharm. Clin. Res.*, 8(2):60-63.
- [11] Christine E., Gruda N. 2015. Urban vegetable for food security in cities. A review. *Agronomy for Sustainable Development Volume* 35(2):483-498. DOI: 10.1007/s13593-014-0273-y.
- [12] David C. Love, Jillian P. Fry, Ximin Li, Elizabeth S. Hill, Laura Genello, Ken Semmense, Richard E. Thompson. 2015. Commercial aquaponics production and profitability: Findings from an international survey. *Aquaculture* 435:67–74.
- [13] Department of Fisheries. 2018. Fisheries Statistical Yearbook of Bangladesh, 2011- 2012, Fisheries Recourses Survey System, Department of Fisheries, Bangladesh, Dhaka (pp. 8-10).
- [14] Endut A., Jusoh A., Ali N., Nik W.W.B. 2011. Nutrient removal from aquaculture wastewater by vegetable production in aquaponics recirculation system. *Journal of Desalination.*; 32:422-430.
- [15] FAO, IFAD, UNICEF, WFP and WHO. 2018. The State of Food Security and Nutrition in the World 2018. Building climate resilience for food security and nutrition. Rome, FAO.
- [16] Food and Agricultural Organization (FAO) of the United Nations. 2012. The State of World Fisheries and Aquaculture, Rome, Italy.
- [17] Ghaly A. E., Snow A. M. 2008. Use of barley for the purification of aquaculture wastewater in a hydroponics system. *American Journal of Environmental Science.*; 4:89-102.
- [18] Giampieri F., Tulipani S., Alvarez-Suarez J. M., Quiles J. L., Mezzetti B., Battino M. 2012. The strawberry: composition, nutritional quality, and impact on human health. *Nutrition*, 28(1):9-19.
- [19] Gul P. 1994. Seasonal variation of oil and Menthol content in *Menthaarvensis* L. *Pakistan journal of forestry*, 44:16-20.
- [20] Hadjlaoui H., Najla T., Emira N., Mejdí S., Hanan F., Riadh K., & Amina B. 2009. *World Journal of Microbiology and Biotechnology*, 25:2227–2238.
- [21] Halvorsen B. L., Carlsen M. H., Phillips K. M., Bøhn S. K., Holte K., Jacobs D.R. Jr, Blomhoff R. 2006. Content of redox-active compounds (ie, antioxidants) in foods consumed in the United States. *Am J. Clin. Nutr.*, 84(1):95-135.
- [22] Hochmuth, R., and G. J. Hochmuth. 2001. A decade of change in Florida's greenhouse vegetable industry: 1991–2001 Pp. 280–283 in *Proc. Fla. State Hort. Soc.*
- [23] HuetM.1972. *TextbookofFishculture:breedingandcultivation of fish*.Fishing news books Ltd., West By-fleet, Surrey, London, England, 400-436.
- [24] Hugh Brammer. 2016. Floods, cyclones, drought and climate change in Bangladesh: a reality check. *International Journal of Environmental Studies* 73(6):1-22.

- [25] Kangas C. P. 2004. ECOLOGICAL ENGINEERING: Principles and Practice. LEWIS PUBLISHERS, A CRC Press Company Boca Raton, London; New York; Washington, D.C.
- [26] Katy Askew. 2019. Vertical farming: A sustainable solution to food insecurity? <https://www.foodnavigator.com/article/2019/01/28/vertical-farming-a-sustainable-solution-to-food-in>.
- [27] Kheir A.K. 2018. The Vertical Farm: A Review of Developments and Implications for the Vertical City-Review. Buildings, 8: 24; doi:10.3390/buildings8020024.
- [28] Kodmany A. K. 2018. The Vertical City: A Sustainable Development Model; WIT Press: Southampton, UK, ISBN 978-1-78466-257-8, p756.
- [29] Liu R. H. 2003. Health benefits of fruit and vegetables are from additive and synergistic combinations of phytochemicals. American Journal of Clinical Nutrition, 78 (3): 517-520.
- [30] Liu W., Chen D. K., and Liu Z. X. 2004. High efficiency column culture system in China. ActaHortic. 691:495-500.
- [31] Liu, T., Yang, M., Han, Z., David W. O. 2016. Rooftop production of leafy vegetables can be profitable and less contaminated than farm-grown vegetables. Agron. Sustain. Dev. 36, 41. <https://doi.org/10.1007/s13593-016-0378-6>.
- [32] Makori, A.J., Abuom, P.O., Kapiyo, R. AnyonaD. N. ; Dida G. O.2017. Effects of water physico-chemical parameters on tilapia (*Oreochromis niloticus*) growth in earthen ponds in Teso North Sub-County, Busia County. Fish Aquatic Sci 20, 30. <https://doi.org/10.1186/s41240-017-0075-7>.
- [33] Marco Ottinger, KerstenClauss, Claudia Kuenzer. 2016. Aquaculture: Relevance, Distribution, Impacts and Spatial Assessments – A Review. Ocean & Coastal Management 119:244-266.
- [34] Midmore D.J., Churilova E., Roy B. 2011. An option for green roof-tops and self- sufficient fresh food production. Rural Industries Research and Development Corporation, 11:67.
- [35] Normala W., Estim A., and Kian A. Y. S. 2010. Producing organic fish and mint in an aquaponics system. A Model of green technology in action, Borneo Marine Research Institute, Sabah, Malaysia. Journal of Aquaponics, 58, 28-31.
- [36] Pandey K. B. and Rizvi S. I. 2009. Plant polyphenols as dietary antioxidants in human health and disease. Oxidative Medicine and Cellular Longevity 2: 270-8.
- [37] Pantanella E., M. Cardarelli, Giuseppe Colla, MarcucciE. R. A. 2012. Aquaponics vs. Hydroponics: Production and Quality of Lettuce Crop. Actahorticulturae, 927(927):887-894. DOI: 10.17660/ActaHortic.2012.927.109.
- [38] Paxton, A. 1994. "The Food Miles Report: The dangers of long-distance food transport". London, UK: SAFE Alliance.
- [39] Rahmatullah R., M. Das and S. M. Rahmatullah. 2010. Suitable stocking density of tilapia in an aquaponics system. Bangladesh. J. Fish. Res., 14(1-2):29-35.
- [40] Rakocy J.E., Bailey D.S.R., Shultz C., and Thoman E.S. 2004. Update on tilapia and vegetable production in the UVI aquaponics system. p. 676-690. In: New Dimensions on Farmed Tilapia: Proceedings of the Sixth International Symposium on Tilapia in Aquaculture, Held September 12-16, 2004 in Manila, Philippines.
- [41] Resh H. M. 2012. Hydroponic food production: a definitive guidebook for the advanced home gardener and the commercial hydroponic grower. CRC Press.
- [42] Sahil K., Sudeep B., and Akanksha M. 2011. Standardization of medicinal plant materials. Institute of Pharmaceutical Sciences and Drug Research, Rajasthan, India. International Journal of Research in Ayurveda and Pharmacy, 2, 1100-1109.
- [43] Salam M. A., Jahan N., Hashem S., Rana K. M. S. 2014. Feasibility of tomato production in aquaponics system using different substrates. Progressive Agriculture, 25:54-62.
- [44] Swingle HS. 1968. Fish kills caused by phytoplankton blooms and their prevention. FAO. Fish Reproduction. 4(5):407-411.
- [45] The USDA National Nutrient Database for Standard Reference. 2011. The Nutrient Data Laboratory, Beltsville Human Nutrition Research Center.
- [46] Tyson RV, Simonne EH, Davis M, Lamb EM, White JM, Treadwell DD. 2007. Effect of nutrient solution, nitrate nitrogen concentration, and pH on nitrification rate in perlite medium. Journal of Plant Nutrition. 30:901-913.
- [47] Uddin M. Taj. and IsratFarjana. 2012. An Economic Study of Low Lying Inland Fish Farming in Selected Areas of Kishoreganj District. Progress. Agric. 23(1 & 2): 81- 90.
- [48] Verma R. S., Rahman L., Verma R. K., Chauhan A., Yadav A. K., and Singh A. 2010. Essential oil composition of menthol mint (*Mentha arvensis*) and pepper mint (*Menthapipertia*) cultivars at different stages of plant growth from Kumanon region, west Himalaya, India. Journal of medicinal and aromatic plants, 1:13-18.
- [49] Wakeland W., Cholette S., Venkat K. 2012 Food transportation issues and reducing carbon footprint. In: Boye J., Arcand Y. (eds) Green Technologies in Food Production and Processing. Food Engineering Series. Springer, Boston, MA.
- [50] Watanabe W., LosordoT., Fitzsimmons K. M. Hanley F. 2002. Tilapia Production Systems in the Americas: Technological Advances, Trends, and Challenges. Reviews in Fisheries Science 10(3):465-498. DOI: 10.1080/20026491051758.
- [51] Werner Kloas, Roman Groß, Daniela Baganz, Johannes Graupner, Henrik Monsees, Uwe Schmidt, Georg Staaks, Johanna Suhl, Martin Tschirner, Bernd Wittstock, Sven Wuertz, Andrea Zikova, Bernhard Rennert.2015. A new concept for aquaponics systems to improve sustainability, increase productivity, and reduce environmental impacts. Aquacult Environ Interact., 7: 179-192.
- [52] Wortman B, Wheaton F. 1991. Temperature effects on biodrum nitrification. Journal of Aquacultural Engineering. 10:183-205.

# Analysis of Air Conditioning Schemes based on Evaporative Cooling of Air using Solar Energy

Toshmamatov B.M.<sup>1</sup>, Temirova L.Z.<sup>2</sup>, Baratova S.R.<sup>3</sup>, Safarova S.U.<sup>4</sup>, Khusunov Sh.Kh.<sup>5</sup>

<sup>1</sup>Assistant, Department of Thermal Power Engineering, Karshi Engineering Economics Institute, Karshi, Uzbekistan

<sup>2,3</sup>3rd year student, Karshi Engineering Economics Institute, Karshi, Uzbekistan

<sup>4,5</sup>2nd year student, Karshi Engineering Economics Institute, Karshi, Uzbekistan

**Abstract**— The article presents the calculation method based on the heat and humidity parameters of the units direct and indirect-evaporative cooling in air conditioning systems in buildings are analyzed various technical diagrams. On the basis of experimental and theoretical studies established the benefits of schemes based on indirect-evaporative cooling. The processes of heat and humidity of air treatment, demonstrate the benefits of solar installations with devices indirect evaporative-type compared to conventional solutions.

**Keywords**— Climate, Air, Compressor, Rotating Heat Exchanger, Irrigation Chamber, Solar Energy, Solar Installation.

## I. INTRODUCTION

To create a comfortable climate for a person in a microclimate in a room, it is necessary to provide air exchange and normalized air parameters. This also applies to most industrial shops in industrial production. Large air exchange in such premises entails and the corresponding heat costs for heating the supply air during the cold period of the year. In the summer, this is also associated with significant energy costs for cooling the air [1,2].

## II. LITERATURE SURVEY

When air blows through a wet medium—a tee shirt, aspen fibers (excelsior), or treated cellulose, fiberglass, or plastic—some of the water is transferred to the air and its dry bulb temperature is lowered. The cooling effect depends on the temperature difference between dry and wet bulb temperatures, the pathway and velocity of the air, and the quality and condition of the medium.

There's a world of difference between old-style swamp coolers and modern evaporative cooling systems. The latter can provide years of trouble-free service and cool, clean, comfortable, fresh air at a lower energy cost than conventional air conditioners—and initial costs are competitive as well. In addition, the latest evaporative cooler designs are a lot easier on the grid than compressor-based cooling systems. Instead of peak demands of three to five kilowatts (kW) or more, typical demands for mid-size evaporative coolers are on the order of one kW. In addition to improved performance, modern evaporative coolers include options for thermostatic control and automated flushing of reservoir water to reduce buildup of impurities.

Accordingly, wide-spread use of evaporative coolers can help delay adding expensive new power plants to the electric grid and the controversial transmission lines that often accompany them. That's the reason a number of utility companies in areas with hot, dry summers and substantial population growth have programs to promote efficient evaporative coolers.

“Direct” evaporative coolers use a fan to pull outside air through media (pads) that are kept thoroughly wet by water that is sprayed or dripped on them (Fig.1). This both filters the air and cools it. The water is typically delivered via tubes from a small pump which draws from a reservoir below. The reservoir is replenished with tap water whose level is controlled by a float valve [3, 4].

The resulting fresh, cool, humidified air is blown into buildings where the pattern of flow (and cool air delivered) is determined by the location and extent of openings in the conditioned envelope such as windows or special dedicated ducts.

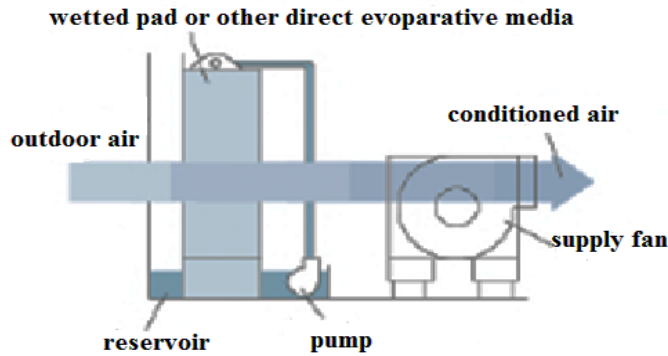


**FIGURE 1. Direct evaporative cooler. Air is pulled across a thoroughly wetted medium as evenly as possible. Lower speeds give more exposure time to the wetted media, thereby achieving more cooling.**

**III. SIGNIFICANCE OF THE SYSTEM**

Currently, one of the ways to reduce the consumption of expensive traditional energy resources in industrial production and in the energy sector is to use renewable energy sources.

With the constant increase in fossil energy prices, as well as the depletion of oil and gas reserves, an increasing number of countries are using alternative(renewable) energy sources [5,6,7,8].

One of the promising ways to reduce the energy intensity of traditional air-conditioning units using compressor refrigerating machines is the use of thermodynamic non-equilibrium air as a renewable energy resource. Systems that use this energy for cold production include direct and indirect evaporative air cooling units [1, 2], which can be successfully used in solar air-conditioning plants. The principle of operation of solar conditioning plants is based on preliminary treatment of air in the adsorption dryer and subsequent cooling of the air flow in a rotating heat exchanger and an irrigation chamber (Fig.2).

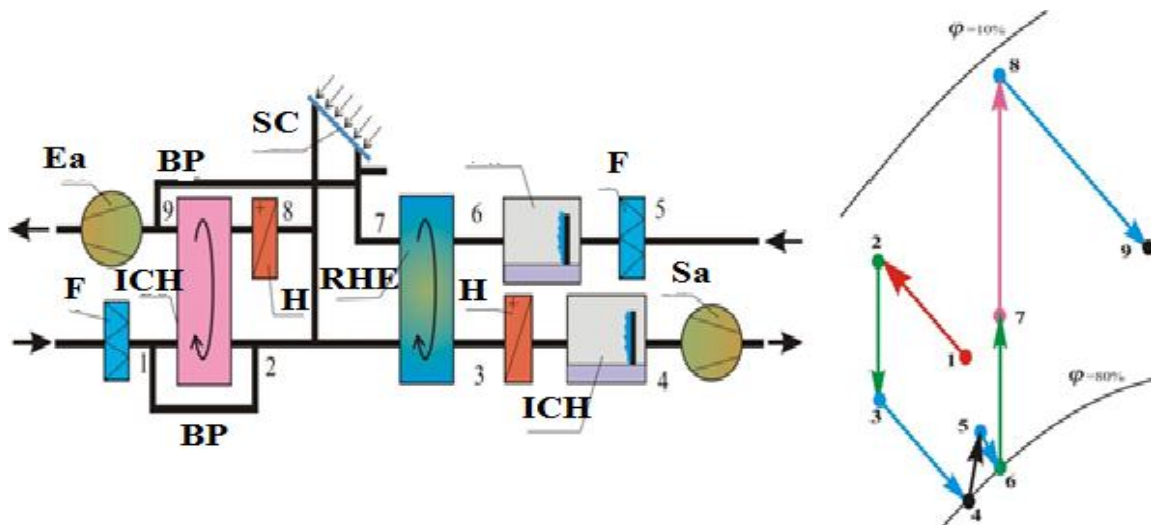


**FIGURE 2: Solar air conditioning installation a) - installation diagram; b) - air processing processes on the i-d diagram: (1-2) - dehumidification of air in the sorbing nozzle; (2-3) - cooling in a rotary heat exchanger; (3-4) - cooling and humidifying in the irrigation chamber; (4-5) - assimilation of heat and moisture in an air-conditioned room; (5-6) - cooling and humidifying the exhaust air flow in the irrigation chamber; (6-7) - preheating the exhaust air in the rotary heat exchanger; (7-8) - heating of the regeneration air in the solar collector and the air heater; (8-9) - humidification and cooling of air in the regeneration sector of the desiccant nozzle.**

**IV. SYSTEM DESIGN**

In Fig. 2 shows the principle of the traditional solar air conditioning system. Pre-cleaned in the filter (P), the outside air with parameters (1) is dried and heated in the sorption nozzle of the rotor (NR) to state (2). After "dry" cooling at constant moisture content (2-3) in the rotary heat exchanger (RHE), the air is adiabatically humidified in the irrigation chamber (ICH)

to state (4) and with these parameters air is supplied to the air-conditioned room, in which it assimilates heat and moisture (4-5). The exhaust air is adiabatically humidified in the irrigation chamber (5-6), after which it is heated (6-7) in a rotating heat exchanger (RHE). The final heating of the air (7-8), going to regeneration of the desiccant nozzle, is carried out in the solar collector (SC) and (with insufficient heating in the solar collector) in the air heater (H). The change in the parameters of the regeneration air in the desiccant nozzle corresponds to the i-d-line diagram (8-9). Part of the exhaust air, not intended for regeneration of the nozzle, is removed through the bypass (BP) into the atmosphere.

## V. DATASET DESCRIPTION

In winter, the air dehumidifier (ICH) is not used, and the external supply air is directed through the bypass directly to the input to the rotating heat exchanger (RHE), which in this case acts as a heat exchanger for the exhaust air [3]. In addition, it is possible to organize the recirculation of exhaust air at the outlet from the solar collector, or, when the situation permits, to partially use outside air for regeneration purposes, which leads to a reduction in energy consumption for air treatment.

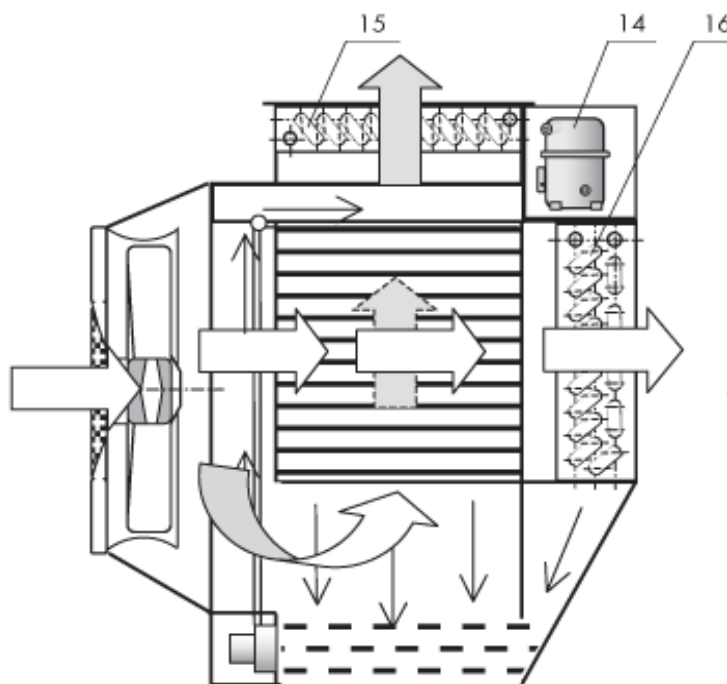


**FIGURE 3: Combined evaporative cooler with XM.**  
14 - compressor XM, 15 - condenser XM, 16 - evaporator XM.

It should be noted that solar conditioning systems, characterized by a sufficiently high efficiency [2], have certain drawbacks. The main drawback is associated with an increase in the relative humidity of the air at the outlet from the irrigation chamber (up to 80-90%), which significantly reduces the assimilative power of the supply air in rooms with a predominance of moisture occurrences. As a result, the conditions of thermal comfort in an air-conditioned room during the summer period may be violated.

In the proposed a number of solutions aimed at eliminating the negative phenomena associated with the humidification of fresh air in the summer, and increasing the efficiency of air cooling by replacing the irrigation chamber with indirect-evaporative devices [3, 4].

Indirect evaporative cooling of air is a process in which air does not have direct contact with water, and its cooling occurs through a heat exchange surface (Fig. 3). Water that absorbs heat evaporates in another stream of air, while its temperature decreases. The flow of air, cooled by water in the absence of direct contact with it, is called the main one, and the airflow in which the evaporation of water taking up this heat from the main stream is auxiliary. In the combined apparatus, the process of cooling the main air flow is carried out in the dry channels of the nozzle with decreasing enthalpy and constant moisture content due to the evaporation of water in adjacent moist channels along which the auxiliary air flow moves [3].

The initial data for calculations based on the developed calculation procedure [4] are given in Table 1.

**TABLE 1**  
**COMPARATIVE INDICATORS OF TWO SYSTEMS**

Indicators	System Type	
	two-stage evaporative cooling	two independent air conditioners KC-25
Performance by air, supplied to the serviced premises, in m <sup>3</sup> /h	20000	10000
The available pressure for the supply duct network in kg/m <sup>2</sup>	30	15
Cooling capacity for assimilation of heat in serviced premises in kkal/h	40320	40000
Total cooling of supply air in kkal/h	126095	50000
Installed power of electric motors for main air conditioners (drive of fans, refrigeration compressors) in kW	12,9	22
The amount of circulating water in the heat exchangers of the first stage or for cooling condensers of refrigerating machines in kg / h	25964	9200
Installed capacity to cool the circulating water in the first stage of the evaporative air-conditioning unit or in the cooling tower for autonomous air conditioners in kW	18,6	8
Total power consumption in the presence of a cooling tower in the scheme of independent air conditioners in kW-h	3150	3000
Capacity per 1000 kcal / h: -by common cooling of supply air -the cooling capacity for assimilation of heat in the premises	0,25 0,785	0,6 0,75

## VI. CONCLUSION AND FUTURE WORK

Thus, the realization of IEC (in contrast to direct evaporative cooling) makes it possible to use the natural thermodynamic non-equilibrium of atmospheric air to produce cold.

The prospects of using these devices in solar air-conditioning plants are due to the possibility:

- Reducing the temperature level of the resulting cold;
- Improving the efficiency of latent heat assimilation in air-conditioned rooms;
- Reducing energy consumption by means of a purposeful combination of different flow patterns of exchanging flows;
- Rational use of heat of phase transformations and renewable energy resources of thermodynamic non-equilibrium of atmospheric air.

Fig.2. presents examples of schemes for processing fresh air in solar air-conditioning plants using the IEC cross-precision apparatus. A qualitative analysis of the proposed schemes was carried out under the following assumptions:

- Air parameters at the outlet from the sorption dryer are assumed to be the same for all options;
- The temperature of the exhaust air is equal to the temperature of the air in the room;
- Depending on the temperature of the air at the outlet of the CRO, the air exchange changes in such a way as to maintain the assimilation capacity of the fresh air, which is constant for all options;
- The efficiency of the regeneration process of the desiccant nozzle is assumed to be the same for all variants.

**REFERENCES**

- [1] Toshmamatov B.M., Shoturaev A.R., Choriev F.A. Experimental studies of the indirect evaporative air conditioning system. Academic Scientific and Methodological Journal. No. 3 (30), 2018. Russia. PP. 17-20.
- [2] Toshmamatov B.M. Two-stage evaporative cooling system for air conditioning systems. Academy Scientific and Methodological Journal No. 3 (18), 2017. Russia. PP. 23-25.
- [3] Chandrakant Wani, Satyashree Ghodke, Chaitanya Shrivastava. A review on potential of Maisotsenko cycle in energy saving applications using evaporative cooling // International journal of advance research in science, engineering and technology. – 2012, - Vol. 1. Issue 1. –p, 15-20.
- [4] Anisimov S., Pandelidis D. Numerical study of the cross-flow heat and mass exchanger for indirect evaporative cooling // Proceedings of the Xth international scientific conference „ Indoor Air and Environment Quality", Budapest, May 13-20. 2012. –p, 149-156.
- [5] B.M.Toshmamatov, G.N.Uzakov, S.R.Baratova.Utilizatsiya tverdix bitovix otxodov s ispolzovaniemsolnechnoy energii. Mejdunarodniynauchnijurnal«Nauchniegorizonti» 2019, №2, ss. 255-260.
- [6] Uzakov G.N., Toshmamatov B.M., Shomuratova S.M.,Temirova L.Z. Calculation of energy efficiency of the solar installation for the processing of municipal solid waste. International Journal of Advanced Research in Science, Engineering and Technology Vol. 6, Issue12, December 2019.
- [7] Toshmamatov B. M, Uzakov G. N, Kodirov I. N & Khatamov I. A. Calculation of the heat balance of the solar installation for the thermal processing of municipal solid waste. International Journal of Applied Engineering Research and Development (IJAERD) ISSN (P): 2250–1584; ISSN (E): 2278–9383 Vol. 10, Issue 1, Jun 2020, 21–30.
- [8] Uzakov G.N., Toshmamatov B.M., Mamedova D.N., Temirova L.Z., Khusunov Sh.Kh. Experimental solar installation for the processing of municipal solid waste. EPRA International Journal of Research and Development (IJRD). Volume: 5 | Issue: 3 | March 2020 . pp. 299-303.



**AD Publications**

**Sector-3, MP Nagar, Bikaner,  
Rajasthan, India**

**[www.adpublications.org](http://www.adpublications.org), [info@adpublications.org](mailto:info@adpublications.org)**